Approximate account of the connected quadruply excited clusters in the coupled-pair many-electron theory

J. Paldus,* J. Čížek,* and M. Takahashi†
Department of Applied Mathematics, University of Waterloo, Waterloo, Ontario, Canada N2L 3G1
(Received 15 June 1984)

In nondegenerate systems, the tetraexcited clusters are well approximated by products of disconnected pair clusters and the connected quadruply excited component is negligible. In contrast, when the reference state becomes quasidegenerate with the lowest biexcited configuration(s), the connected quadruply excited clusters become very important. To extend the applicability of the coupled-pair many-electron theory to such situations, we approximate the connected tetraexcited contribution in the form suggested by the unrestricted Hartree-Fock-type wave function, or one of its projected versions, such as the alternant molecular-orbital method. We show that the incorporation of the connected quadruply excited clusters into the coupled-pair equations effectively cancels certain nonlinear terms, originating from disconnected quadruple excitations, so that the resulting equations are very similar (up to a numerical factor) to the approximate coupled-pair theory, in which only those nonlinear terms which factorize with respect to the hole-electron pairs are considered. This fact shows in turn why various approximate coupled-pair approaches can often provide better results than the full coupled-pair many-electron theory.

I. INTRODUCTION

The coupled-cluster (CC) approach to the many-fermion correlation problem is nowadays widely used in applications to both many-nucleon and many-electron systems. Though the technical aspects of nuclear or atomic, molecular, and solid-state applications may be vastly different, the structure of the CC equations and formalism as well as basic philosophy are essentially the same, namely, to get proper dependence on particle number (size extensivity).

The exponential structure of the many-body wave function was first recognized by Hubbard[1] and its exploitation in the form of the cluster expansion *Ansatz* was first suggested by Coester and Kümmel.[2] Designating the exact and the independent particle model (IPM) states of an N-fermion system as $|\Psi\rangle$ and $|\Phi_0\rangle$, respectively, this *Ansatz* takes the form

$$|\Psi\rangle=\exp(\hat{T})|\Phi_0\rangle\ , \tag{1}$$

where the cluster operator $\hat{T}$ is given by the sum of its i-particle components $\hat{T}_i$,

$$\hat{T}=\sum_{i=1}^{N}\hat{T}_i\ . \tag{2}$$

In contrast to the shell model or configuration-interaction (CI) *Ansatz*, which is linear in i-times-excited configurations,

$$|\Psi\rangle=\hat{C}|\Phi_0\rangle,\quad \hat{C}=\sum_{i=1}^{N}\hat{C}_i\ , \tag{3}$$

where again $\hat{C}_i$ is the i-fold excitation operator yielding a linear combination of i-times-excited configuration states when acting on the IPM reference state $|\Phi_0\rangle$, the exponential cluster expansion *Ansatz* (1) is physically better motivated yielding the correct particle number N dependence even when $\hat{T}$ is truncated to low-order excitations. In more modern parlance, this behavior is often referred to as the size extensivity or size consistency (the latter also assumes that $|\Phi_0\rangle$ correctly dissociates) of the CC approach. A simple comparison[3] of both *Ansätze*, Eqs. (1) and (3), yields the well-known relationship between the CI excitation operators $\hat{C}_i$ and the cluster operators $\hat{T}_i$, namely

$$\hat{C}_i=\hat{T}_i+\hat{Q}_i\ , \tag{4}$$

where

$$\hat{Q}_i=\sum_{\mathscr{P}_i}\prod_{j=0}^{i-1}(r_j!)^{-1}\hat{T}_j^{r_j} \tag{5}$$

represents the so-called disconnected ith-order cluster component of $\hat{C}_i$. The sum extends over all nontrivial partitions $\mathscr{P}_i$ of i,

$$\sum_{j=1}^{i-1}jr_j=i,\quad 0\le r_j\le i;\quad \hat{T}_j^0=\hat{1} \tag{6}$$

so that physically $\hat{Q}_i$ represents i-fold excitations which are decomposable into the products of lower-order independent excitations.

For the nondegenerate ground state of pairwise interacting fermions, the so-called pair clusters $\hat{T}_2$ represent by far the most important contribution to $\hat{T}$. In fact, the correlation energy of such systems is completely determined by the $\hat{T}_1$ and $\hat{T}_2$ cluster components. With an appropriate choice (maximum overlap or Brueckner orbitals) of the IPM reference state $|\Phi_0\rangle$, the monoexcited clusters exactly vanish and even with the usually em-

ployed Hartree-Fock (HF) reference state, they are quite negligible. In any case, these clusters can be easily accounted for even when a nonstandard reference state is used, as for example in localized approaches,[4] since their number is small. Thus, in most instances we have that $\hat{C}_2 \approx \hat{T}_2$ and $\hat{T}_1 \approx 0$. In contrast, the tetraexcited cluster contribution, whose role is next in importance to the biexcited clusters, comes via their direct interaction with pair clusters, and is normally due to the disconnected component, so that $\hat{C}_4 \approx \frac{1}{2}\hat{T}_2^2$, since

$$\hat{T}_4 \ll \tfrac{1}{2}\hat{T}_2^2 , \tag{7}$$

at least in nonmetallic systems. This fact enables us to truncate the cluster components in Eq. (2) at $\hat{T}_2$ (or $\hat{T}_3$, which are usually next in importance to the $\frac{1}{2}\hat{T}_2^2$ contribution) rather than at the $\hat{C}_4$ level of the standard CI approach. Even when truncating at the $\hat{T}_2$ level, all higher excited disconnected components are accounted for through the exponential *Ansatz* (1).

The explicit form of the equations determining cluster components $\hat{T}_i$ was first given in Ref. 5. Their derivation exploited time-independent diagrammatic formalism (see also Ref. 6) related to that of many-body perturbation theory (MBPT). The explicit algebraic form, which was given for the most important pair cluster approximation, was particularly suitable for the applications to atomic and molecular problems. These coupled-pair equations were also derived using an ordinary wave-function formalism.[7] During the last decade other derivations and extensions of the CC formalism appeared as well as new developments of efficient computational implementation of this approach, especially for the molecular electronic correlation problem. Presently, numerous review articles and parts of monographs exist which outline these various developments and we list the most recent ones in Refs. 8–14. Those developments which are particularly relevant to this paper will now be briefly reviewed.

The CC equations are most simply derived by substituting the cluster expansion *Ansatz*, Eq. (1), into the time-independent Schrödinger equation, which yields

$$\{[\hat{H}_N \exp(\hat{T})]_C - \Delta\epsilon\} \mid \Phi_0\rangle = 0 . \tag{8}$$

Here we exploit the normal product form (with respect to the hole-particle vacuum $\mid \Phi_0\rangle$, cf. Refs. 5, 6, and 15) of the Hamiltonian, $\hat{H}_N$, and designate the connected part by the subscript C. Projecting this equation onto the reference state $\mid \Phi_0\rangle$ we obtain the expression for the energy $\Delta\epsilon$ (relative to the reference state energy)

$$\Delta\epsilon = \langle \Phi_0 \mid \hat{H}_N(\tfrac{1}{2}\hat{T}_1^2 + \hat{T}_2) \mid \Phi_0\rangle , \tag{9}$$

assuming that the Hamiltonian contains at most two-particle terms. Projecting then Eq. (8) onto the selected configurations which span $\{\hat{T}_i \mid \Phi_0\rangle\}$, $i \leq n$, yields nonlinear algebraic equations determining the cluster components $\hat{T}_i$, $i \leq n$, assuming of course that the higher excited clusters $\hat{T}_i$, $i > n$, are neglected. The explicit spin-orbital form of these equations is best obtained by using the diagrammatic methods based on Wick's theorem and Feynman-like diagrams.[5,6,15] The most common coupled-pair formalism corresponds to the double excitation cutoff and is referred to as the coupled-pair many-electron theory (CPMET) or more succinctly as the CCD (coupled clusters with doubles) approach or CCSD approach when singly excited clusters are included as well.

For a spin-independent Hamiltonian the CC equations can be simplified by eliminating the spin variables. The resulting spin-free orbital formalism is referred to as spin-adapted CC approach. A standard spin-adapted orbital form of the CC equations can be easily obtained by replacing the spin-orbital labels by the orbital ones and by assigning the factor of 2 to each closed loop of fermion lines[5,6] (for the two possible spin orientations). In terms of many-electron configurations, this spin adaptation can be shown to correspond to the use of spin-bonded functions, which are generally nonorthogonal (moreover, for clusters higher than biexcited, this simple spin-elimination procedure leads to a linearly dependent set of configurations).[16] Combining the time-independent diagrammatic technique[15] with spin algebraic graphical methods[17] we can obtain orthogonally spin-adapted formalism.[18,19] The most convenient coupling scheme, at least for the pair clusters $\hat{T}_2$, is the so-called *pp-hh* scheme,[18,20] in which case the hole spins are first coupled independently of the particle spins into the intermediate hole and particle spin states, respectively, which are then coupled into the final spin (which in the closed-shell ground-state case considered is the singlet spin state). The orthogonally spin-adapted formalism is not only convenient computationally, since the required matrices are sparser,[21] and enables one to cast the CC formalism into the SCEP (self-consistent electron pair) form as shown by Chiles and Dykstra[22] but, as we shall see below, it is also essential for the developments presented in this paper.

We must also mention at this point various approximate coupled-pair (ACP) approaches. Neglecting the nonlinear terms in the CC(S)D equations we obtain the corresponding linear approximation designated as L-CPMET or L-CC(S)D. This approximation is still size extensive, in contrast to the corresponding variational CI procedure restricted to biexcited configurations, (D-CI), and is equivalent to the infinite-order MBPT restricted to the diagrams with at most biexcited intermediate states [thus also called DMBPT (∞) (Ref. 23)]. This approximation yields excellent results as long as no quasidegeneracy is present. It can also be related with the often employed Davidson correction.[24] A study of the role of the nonlinear terms in the CCD equations revealed that the diagrams which do not factorize relative to the hole pair can be neglected.[25] This observation was made independently by several investigators[21,26–28] and its remarkable performance was verified on a number of systems both at the semiempirical and *ab initio* levels. We refer to this approach as the ACP-D45 approximation (since only diagrams 4 and 5 of Fig. 3 of Ref. 18 are considered in the nonlinear part) or, for short, as the ACP approximation. There also exists a multitude of yet more drastic approximations, which are generally referred to as CEPA(n) (coupled-electron-pair approximation) approaches. These approaches, which can be identified as versions of the

ACP approximation, where only certain EPV (exclusion principle violating) diagrams are retained, have been widely employed.[29–32] More detailed outline of the relationship of these approaches with the ACP approach as well as examples of their performance can be found in Ref. 26.

Numerous applications of the CC formalism to various atomic and molecular systems have clearly shown that the CCD or CCSD approach can provide very accurate correlation energies provided that the ground state considered is not quasidegenerate. The correlation energy obtained with the CCSD approach is practically identical with that resulting from the CI limited to singly, doubly, and quadruply excited configurations.[8,16,33] The remaining error usually does not exceed 3% of the correlation energy and is primarily due to the triexcited configurations. The latter can be accounted for by including the $\hat{T}_3$ component clusters either exactly[16,33] or in an approximate manner via finite-order perturbation theory (CCSDT and various approximate versions).[8]

The CCD or CCSD approach can also yield very good results in certain quasidegenerate situations, particularly in the case of the so-called orbital quasidegeneracy[34,35] which arises due to the proximity of the highest occupied and the lowest unoccupied levels (e.g., $2s$-$2p$ quasidegeneracy in the Be atom) but which causes only a slight mixing of the ground state and the lowest biexcited configurations. A remarkable performance of the CC(S)D approach was found not only for the Be atom[21,27] but, in fact, for the entire Be isoelectronic series.[35] In the case of the state or configurational quasidegeneracy,[34] when the ground-state configuration is heavily mixed with the lowest biexcited configuration while the highest occupied and lowest unoccupied one-electron levels remain well separated, the CCD approach still provides a very reasonable approximation as we showed in model studies of various H_4 systems.[26,36] Nevertheless, the performance of the CCD approach necessarily deteriorates when the quasidegeneracy becomes appreciable, since the basic assumption (7) becomes violated. Only when the $\hat{T}_4$ energy contribution (via the interaction with $\hat{T}_2$ clusters) remains relatively small, as is the case for a few electron systems, the CCSD will provide a still acceptable approximation. However, when the $\hat{T}_4$ contribution becomes essential, as is certainly the case in metalliclike large or extended systems, the CCSD approximation will fail completely.

The importance of the $\hat{T}_4$ clusters was shown directly for the case of linear metal-like systems as modeled by the cyclic polyenes C_NH_N, $N=4\nu+2$, $\nu=1,2,\ldots$. The cluster analysis of the full CI wave functions for the first two members ($N=6$ and 10) shows[37] a very important $\hat{T}_4$ contribution in the strongly correlated limit (large coupling constant). For large systems the same situation can be expected to occur even for intermediate metallic densities. In fact, the CCD approach (which in this case is equivalent to the CCSD approach since $\hat{T}_1$ vanishes by the symmetry), while yielding over 97% of the correlation energy in both intermediate and weakly correlated regions, leads to about a 100% error in the strongly correlated limit of the C_6H_6 model and about a factor of 10 error for the $C_{10}H_{10}$ in the same limit.[34,38,39] For higher members we were unable to find any solution of the CCD equations in this limit and starting with $C_{26}H_{26}$, no solution was found even for spectroscopic parametrization corresponding to physical densities.[38,39] The details of this investigation will be given elsewhere.[38]

The principal aim of this paper is to investigate the possibility of accounting for the $\hat{T}_4$ contribution in the CC formalism. The direct inclusion of the $\hat{T}_4$ clusters in the CC formalism is computationally hardly feasible in the foreseeable future, even for relatively small systems. On the other hand, we show that an approximate account of $\hat{T}_4$ clusters is not only possible, but in fact results in a formalism which is as easy to carry out as the ACP-D45 approach. These developments will also show the ACP approaches in the new light and will provide an understanding for their remarkable success.

II. BASIC CC FORMALISM

We first briefly outline the orthogonally spin-adapted CC formalism[18] in order to introduce the necessary notation and concepts. We shall employ the mixed Hugenholtz-Goldstone diagrams, representing the cluster components by the former and the two-particle part of the Hamiltonian by the latter diagrams in order to obtain the resulting expressions in terms of standard, nonantisymmetrized, two-electron integrals.[15] However, following Brandow,[6,40] the Hugenholtz vertices will be also represented in Goldstone form in order to fix uniquely the phases.[6,18]

We consider the ground state of a closed-shell $N(=2n)$-electron system described by a spin-independent Hamiltonian involving at most two-body scalar potentials $\hat{V}$. Using the second quantization formalism we write this Hamiltonian in the normal product form with respect to the IPM reference state $|\Phi_0\rangle$ regarded as the Fermi vacuum (cf. Ref. 15)

$$\begin{aligned}\hat{H}_N &= \hat{F}_N + \hat{V}_N \\ &= \sum_{a,b} \langle a|\hat{f}|b\rangle \sum_{\sigma} N[\hat{X}^{\dagger}_{a\sigma}\hat{X}_{b\sigma}] \\ &\quad + \tfrac{1}{2} \sum_{a,b,c,d} \langle ab|\hat{v}|cd\rangle \sum_{\sigma,\tau} N[\hat{X}^{\dagger}_{a\sigma}\hat{X}^{\dagger}_{b\tau}\hat{X}_{d\tau}\hat{X}_{c\sigma}] ,\end{aligned} \tag{10}$$

where the one-electron part has the form

$$\langle a|\hat{f}|b\rangle = \langle a|\hat{z}|b\rangle + \sum_{c_1} (2\langle ac_1|\hat{v}|bc_1\rangle - \langle ac_1|\hat{v}|c_1b\rangle) . \tag{11}$$

Here $\hat{X}_{a\sigma}$ ($\hat{X}^{\dagger}_{a\sigma}$) designates the annihilation (creation) operator associated with the IPM spin-orbital basis $\{|A\rangle \equiv |a\rangle|\sigma\rangle\}$. We use capitals to label the spin orbitals and the lower-case letters to designate corresponding orbitals while the spin states are labeled by the lower-case Greek letters. The hole (occupied) and particle (unoccupied) one-electron states with respect to the reference state $|\Phi_0\rangle$ are distinguished by subscripts and superscripts, or

by single and double primes, respectively. No subscripts or superscripts are used when either the hole or particle states are involved.

The i-times-excited cluster operator $\hat{T}_i$ has then the form

$$\hat{T}_i=(i!)^{-1}\sum_{\{A^i\}}\sum_{\{A_i\}}\langle A^1A^2\cdots A^i\,|\,\hat{t}_i\,|\,A_1A_2\cdots A_i\rangle \times\prod_{j=1}^{i}(\hat{X}^\dagger_{A^j}\hat{X}_{A_j})$$

$$=(i!)^{-2}\sum_{\{A^i\}}\sum_{\{A_i\}}\langle A^1\cdots A^i\,|\,\hat{t}_i\,|\,A_1\cdots A_i\rangle_A \times\prod_{j=1}^{i}(\hat{X}^\dagger_{A^j}\hat{X}_{A_j})\,, \tag{12}$$

where $\{A^i\}$ and $\{A_i\}$ represent the sets of summation labels $\{A^1,A^2,\ldots,A^i\}$ and $\{A_1,A_2,\ldots,A_i\}$ and the summation extends over the particle and hole one-particle states, respectively. In the second expression the antisymmetrized $\hat{t}_i$ matrix elements are used, which are defined by

$$\langle A^1A^2\cdots A^i\,|\,\hat{t}_i\,|\,A_1A_2\cdots A_i\rangle_A =\sum_{P\in\mathcal{S}_i}(-1)^p\langle A^1A^2\cdots A^i\,|\,\hat{t}_i\,|\,A_{p_1}A_{p_2}\cdots A_{p_i}\rangle\,, \tag{13}$$

where the summation extends over all $i!$ permutations P of the symmetric group S_i,

$$P=\begin{bmatrix}1, & 2,\ldots, & i\\ p_1, & p_2,\ldots, & p_i\end{bmatrix}, \tag{14}$$

and where p designates the parity of P.

The orthogonally spin-adapted connected biexcited component of the exact wave function $|\Psi\rangle$, Eq. (1), given by $\hat{T}_2\,|\,\Phi_0\rangle$, can be written as follows:[18]

$$\hat{T}_2\,|\,\Phi_0\rangle=\tfrac{1}{4}\sum_{S,M_s}\sum_{S_{21},S^{12}}\sum_{a^1,a^2}\sum_{a_1,a_2}N_a^{-2}\langle a^1a^2\,|\,\hat{t}_2(S,M_s)\,|\,a_1a_2\rangle^{S^{12}}_{S_{21}}\left|\begin{matrix}a^1 & a^2\\ a_1 & a_2\end{matrix};\,SM_s\right\rangle_{S_{21}}^{S^{12}}, \tag{15}$$

using the *pp-hh* spin-adapted states

$$\left|\begin{matrix}a^1 & a^2\\ a_1 & a_2\end{matrix};\,SM_s\right\rangle_{S_{21}}^{S^{12}}=N_a([S]/[S^{12}])^{1/2}\sum_{\sigma_1,\sigma_2,\sigma^1,\sigma^2}\sum_{\sigma_{21},\sigma^{12}}\langle\tfrac{1}{2}\sigma_2\tfrac{1}{2}\sigma_1\,|\,S_{21}\sigma_{21}\rangle\langle\tfrac{1}{2}\sigma^1\tfrac{1}{2}\sigma^2\,|\,S^{12}\sigma^{12}\rangle \times\langle SM_sS_{21}\sigma_{21}\,|\,S^{12}\sigma^{12}\rangle\left|\begin{matrix}a^1\sigma^1 & a^2\sigma^2\\ a_1\sigma_1 & a_2\sigma_2\end{matrix}\right\rangle, \tag{16}$$

where $\langle l_1m_1l_2m_2\,|\,l_3m_3\rangle$ are the Clebsch-Gordan coefficients, and

$$[S]\equiv 2S+1\,. \tag{17}$$

The spin-orbital configurations are defined as follows:

$$\left|\begin{matrix}A^1A^2\cdots A^i\\ A_1A_2\cdots A_i\end{matrix}\right\rangle=\left[\prod_{j=1}^{i}(\hat{X}^\dagger_{A^j}\hat{X}_{A_j})\right]|\,\Phi_0\rangle\,, \tag{18}$$

and the factor N_a,

$$N_a=[(1+\langle a_1\,|\,a_2\rangle)(1+\langle a^1\,|\,a^2\rangle)]^{-1/2}\,, \tag{19}$$

assures the normalization in case the hole and/or particle states involve the same orbital.

Explicitly, designating the six relevant biexcited Slater determinants (18) as G_i $(i=1,\ldots,6)$,[20]

$$G_1=\left|\begin{matrix}a^1\beta & a^2\beta\\ a_1\beta & a_2\beta\end{matrix}\right\rangle=|\cdots a_1\bar{a}^1\cdots a_2\bar{a}^2\cdots|\,,$$

$$G_2=\left|\begin{matrix}a^1\alpha & a^2\alpha\\ a_1\alpha & a_2\alpha\end{matrix}\right\rangle=|\cdots a^1\bar{a}_1\cdots a^2\bar{a}_2\cdots|\,,$$

$$G_3=\left|\begin{matrix}a^1\beta & a^2\alpha\\ a_1\beta & a_2\alpha\end{matrix}\right\rangle=|\cdots a_1\bar{a}^1\cdots a^2\bar{a}_2\cdots|\,, \tag{20}$$

$$G_4=\left|\begin{matrix}a^1\alpha & a^2\beta\\ a_1\alpha & a_2\beta\end{matrix}\right\rangle=|\cdots a^1\bar{a}_1\cdots a_2\bar{a}^2\cdots|\,,$$

$$G_5=\left|\begin{matrix}a^1\beta & a^2\alpha\\ a_1\alpha & a_2\beta\end{matrix}\right\rangle=|\cdots\bar{a}^1\bar{a}_1\cdots a_2a^2\cdots|\,,$$

$$G_6=\left|\begin{matrix}a^1\alpha & a^2\beta\\ a_1\beta & a_2\alpha\end{matrix}\right\rangle=|\cdots a_1a^1\cdots\bar{a}^2\bar{a}_2\cdots|\,,$$

we obtain the following explicit form for the $M_S=0$ *pp-hh* spin-adapted states (16):

$$\begin{aligned}
|\,0\rangle_0^0&=-\tfrac{1}{2}(G_3+G_4-G_5-G_6)\,,\\
|\,0\rangle_1^1&=(1/\sqrt{12})(2G_1+2G_2+G_3+G_4+G_5+G_6)\,,\\
|\,1\rangle_0^1&=\tfrac{1}{2}(G_3-G_4-G_5+G_6)\,,\\
|\,1\rangle_1^0&=\tfrac{1}{2}(G_3-G_4+G_5-G_6)\,,\\
|\,1\rangle_1^1&=(1/\sqrt{2})(G_1-G_2)\,,\\
|\,2\rangle_1^1&=(1/\sqrt{6})(G_1+G_2-G_3-G_4-G_5-G_6)\,,
\end{aligned} \tag{21}$$

where we used the shorthand notation

$$\left|\begin{matrix}a^1 & a^2\\ a_1 & a_2\end{matrix};\,S0\right\rangle_{S_{21}}^{S^{12}}\equiv|\,S\rangle_{S_h}^{S_p}$$

and assumed that $a^1 \neq a^2$, $a_1 \neq a_2$, so that $N_a = 1$. For the singlet case $S = 0$ we simplify our notation by defining

$$\left|\begin{matrix} a^1 & a^2 \\ a_1 & a_2 \end{matrix}\right\rangle_{S_i} \equiv \left|\begin{matrix} a^1 & a^2 \\ a_1 & a_2 \end{matrix}; 00\right\rangle_{S_i}^{S_i} , \tag{22}$$

and note the following desirable properties of singlet *pp-hh* coupled states:

$$\left|\begin{matrix} a^1 & a^2 \\ a_1 & a_2 \end{matrix}\right\rangle_{S_i} = (-1)^{S_i} \left|\begin{matrix} a^1 & a^2 \\ a_2 & a_1 \end{matrix}\right\rangle_{S_i} = \left|\begin{matrix} a^2 & a^1 \\ a_2 & a_1 \end{matrix}\right\rangle_{S_i} . \tag{23}$$

Consequently, when the hole and/or particle labels are identical, the $S_i = 1$ (intermediate triplet coupled) state vanishes leaving only one nonvanishing singlet configuration.

The symmetry-adapted $\hat{t}_2$ matrix elements, associated with orthogonal spin-adapted *pp-hh* coupled states (16), are related with the standard $\hat{t}_2$ matrix elements, Eq. (12), by the same orthogonal transformation as the spin-adapted states (16) are related with spin-orbital configurations (18), namely

$$\langle a^1 a^2 | \hat{t}_2(S,M_s) | a_1 a_2 \rangle_{S_{21}}^{S^{12}} = N_a([S]/[S^{12}])^{1/2} \sum_{\sigma_1,\sigma_2,\sigma^1,\sigma^2} \sum_{\sigma_{21},\sigma^{12}} \langle \tfrac{1}{2}\sigma_2 \tfrac{1}{2}\sigma_1 | S_{21}\sigma_{21} \rangle \langle \tfrac{1}{2}\sigma^1 \tfrac{1}{2}\sigma^2 | S^{12}\sigma^{12} \rangle \times \langle SM_s S_{21}\sigma_{21} | S^{12}\sigma^{12} \rangle \langle a^1\sigma^1 a^2\sigma^2 | \hat{t}_2 | a_1\sigma_1 a_2\sigma_2 \rangle_A . \tag{24}$$

From now on we shall only consider the singlet components so that always $S = M_S = 0$ and $S^{12} = S_{21} = S_i$. We shall further simplify our notation by representing the orbital labels a^i and a_i by their superscripts or subscripts i, distinguishing the particle and hole states by double and single primes, respectively (thus following the notational convention used in Ref. 16), and by dropping the subscript i on the intermediate spin label S_i. We shall thus designate the pertinent $\hat{t}_2$ matrix elements as

$$\langle 1''2'' | \hat{t}_2 | 1'2' \rangle_S \equiv \langle a^1 a^2 | \hat{t}_2 | a_1 a_2 \rangle_S \equiv \langle a^1 a^2 | \hat{t}_2(0,0) | a_1 a_2 \rangle_S^S , \tag{25}$$

so that

$$(\hat{T}_2 | \Phi_0\rangle)_{S=0} = \tfrac{1}{4} \sum_{S=0}^{1} \sum_{1'',2''} \sum_{1',2'} N_a^{-2} \langle 1''2'' | \hat{t}_2 | 1'2' \rangle_S \times \left|\begin{matrix} 1'' & 2'' \\ 1' & 2' \end{matrix}\right\rangle_S , \tag{26}$$

with N_a given by Eq. (19), i.e., $N_a^{-2} = (1 + \langle 1' | 2' \rangle)(1 + \langle 1'' | 2'' \rangle)$. The symmetry-adapted matrix elements, Eq. (25), possess the same symmetric properties as the corresponding *pp-hh* coupled states, namely

$$\langle 1''2'' | \hat{t}_2 | 1'2' \rangle_S = (-1)^S \langle 1''2'' | \hat{t}_2 | 2'1' \rangle_S = \langle 2''1'' | \hat{t}_2 | 2'1' \rangle_S , \tag{27}$$

and

$$\langle 1''2'' | \hat{t}_2 | 1'1' \rangle_1 = \langle 1''1'' | \hat{t}_2 | 1'2' \rangle_1 = \langle 1''1'' | \hat{t}_2 | 1'1' \rangle_1 = 0 . \tag{27'}$$

It is also convenient to define un-normalized matrix elements

$$\langle 1''2'' | \hat{\tau}_2 | 1'2' \rangle_S = N_a^{-1} \langle 1''2'' | \hat{t}_2 | 1'2' \rangle_S , \tag{28}$$

which we shall associate with T_2 vertices in our orbital diagrams, while all the spin-coupling coefficients will be represented by corresponding spin diagrams,[18] as we shall indicate shortly.

In nonorthogonally spin-adapted standard form the orbital $\hat{t}_2$ matrix elements are defined as

$$\langle A^1 A^2 | \hat{t}_2 | A_1 A_2 \rangle = \langle a^1 a^2 | \hat{t}_2 | a_1 a_2 \rangle \langle \sigma^1 | \sigma_1 \rangle \langle \sigma^2 | \sigma_2 \rangle , \tag{29}$$

and are related with the orthogonally spin-adapted matrix elements (24) by

$$\langle 1''2'' | \hat{t}_2 | 1'2' \rangle_S = -N_a[S]^{1/2} \{ (-1)^S \langle 1''2'' | \hat{t}_2 | 1'2' \rangle + \langle 1''2'' | \hat{t}_2 | 2'1' \rangle \} , \tag{30}$$

or, conversely,

$$\langle 1''2'' | \hat{t}_2 | 1'2' \rangle = \tfrac{1}{2} N_a^{-1} (- \langle 1''2'' | \hat{t}_2 | 1'2' \rangle_0 + 3^{-1/2} \langle 1''2'' | \hat{t}_2 | 1'2' \rangle_1) . \tag{31}$$

The diagrammatic representation for the biexcited cluster components, Eq. (26), is achieved by using the pair of diagrams: the orbital diagram of Fig. 1(a) and the corre-

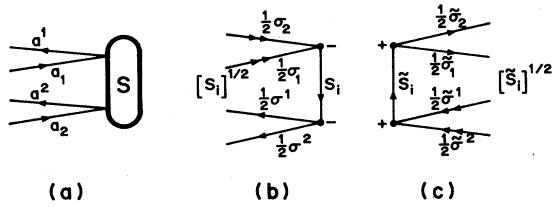

FIG. 1. The orbital (a) and spin (b) diagrams representing the orthogonally spin-adapted biexcited cluster component $\hat{T}_2$. For the orbital diagram we use the so-called Brandow form, i.e., one Goldstone version of Hugenholtz diagram. The spin diagram (b) is the Jucys-type diagram representing the *pp-hh* coupling scheme, Eq. (24), to the resulting singlet ($S_{21} = S^{12} = S_i$) in the 3-*jm* representation (for more details see Ref. 18). The spin diagram (c) is dual to the diagram (b) which is associated with the projection onto the corresponding singlet spin-adapted state (22). Finally, $[S] \equiv 2S + 1$, Eq. (17).

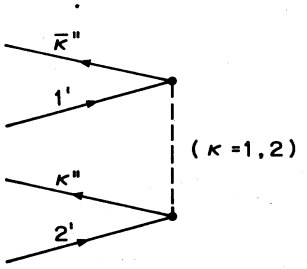

FIG. 2. The resulting orbital diagrams ($\kappa=1,2$), containing no T_2 vertices, and obtained by projecting Eq. (8) onto the doubly excited state (22), $S_i \equiv \tilde{S}$. The contribution of these diagrams to the CCD equations (32) or (41), yielding the absolute term, is given by $\Lambda^{(0)}$, Eq. (35).

sponding spin diagram, Fig. 1(b), representing the *pp-hh* coupling, Eq. (24), into the resulting singlets (see Ref. 18 for details). For the projection onto the corresponding bra states [recall Eq. (8) and the following discussion] we also need the dual spin graph of Fig. 1(c). For more details the reader is referred to Refs. 18–20. The desired CCD equations[41] are then obtained by projecting the Schrödinger equation (8) onto the biexcited states

$$|\Phi_i^{(2)}\rangle \equiv \left| \begin{matrix} 1'' & 2'' \\ 1' & 2' \end{matrix} \right\rangle_{\tilde{S}} ,$$

Eqs. (22) and (16), obtaining

$$\sum_{j=0}^{3} \Lambda^{(j)}(1''2'',1'2';\tilde{S})=0 , \tag{32}$$

where

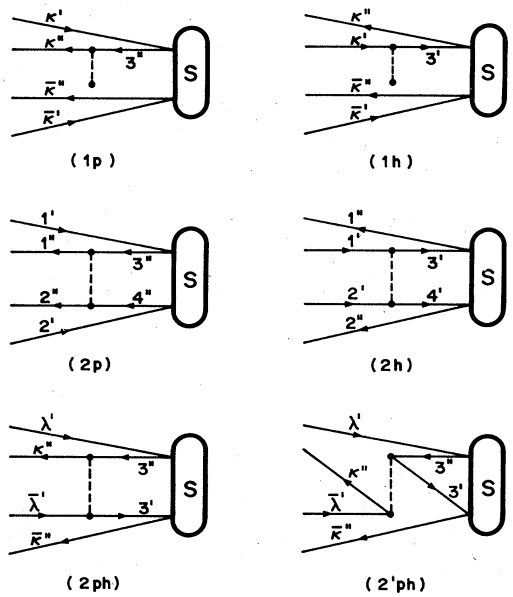

FIG. 3. The resulting orbital diagrams ($\kappa,\lambda=1,2$), containing one T_2 vertex, and obtained by projecting Eq. (8) onto the doubly excited state (22), $S_i \equiv \tilde{S}$. These diagrams contribute the linear terms $\Lambda^{(1)}$, Eq. (36), to the CCD equations (32) or (41). See Eq. (39) for the definition of $\bar{\kappa}$ and $\bar{\lambda}$.

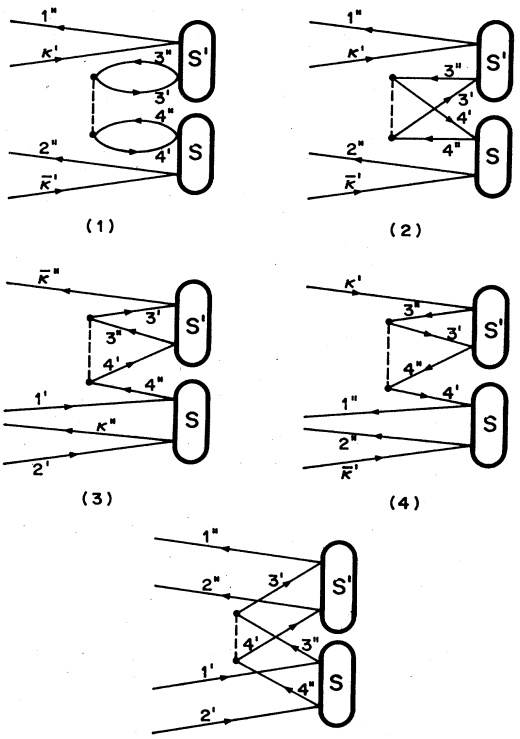

FIG. 4. The resulting orbital diagrams ($\kappa=1,2$), containing two T_2 vertices, and obtained by projecting Eq. (8) onto the doubly excited state (22), $S_i \equiv \tilde{S}$. These diagrams contribute the bilinear term $\Lambda^{(2)}$, Eqs. (37) and (38), to the CCD equations (32) or (41).

$$\Lambda^{(j)}=\frac{1}{j!}\langle \Phi_i^{(2)} | \hat{H}_N \hat{T}_2^j | \Phi_0 \rangle_C, \quad j=0,1,2 \tag{33}$$

and

$$\Lambda^{(3)}=\langle \Phi_i^{(2)} | \hat{H}_N \hat{T}_4 | \Phi_0 \rangle_C . \tag{34}$$

This last $\Lambda^{(3)}$ component is of course neglected in the CCD (or CCSD) approximation in view of the inequality (7), thus decoupling the pair equations from equations for higher cluster components. Explicit expressions in terms of one- and two-electron integrals for the absolute, linear, and bilinear components $\Lambda^{(j)}$, $j=0$, 1, and 2, respectively, are then most easily obtained by applying the diagrammatic technique.[15,20] The relevant orbital diagrams are shown in Figs. 2, 3, and 4 and the corresponding spin diagrams can be found in Ref. 18. The resulting explicit expressions which one obtains by evaluating these diagrams are given below:[18]

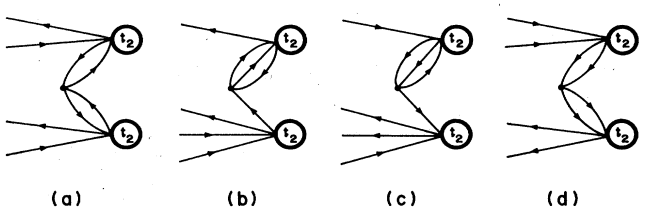

FIG. 5. Resulting Hugenholtz diagrams associated with the nonlinear CCD terms. (a) corresponds to diagrams (1) and (2) of Fig. 4, while (b), (c), and (d) correspond to diagrams 3, 4, and 5, respectively, of the same figure.

$$\Lambda^{(0)}(1''2'',1'2';\tilde{S})=-[\tilde{S}]^{1/2}\{\langle 1''2''\,|\,\hat{v}\,|\,2'1'\rangle+(-1)^{\tilde{S}}\langle 1''2''\,|\,\hat{v}\,|\,1'2'\rangle\}\ , \tag{35}$$

$$\begin{aligned}\Lambda^{(1)}(1''2'',1'2';\tilde{S})=&\sum_{\kappa=1}^{2}\left[\sum_{3''}\langle\kappa''\,|\,\hat{f}\,|\,3''\rangle\langle 3''\bar{\kappa}''\,|\,\hat{\tau}_2\,|\,\kappa'\bar{\kappa}'\rangle_{\tilde{S}}-\sum_{3'}\langle 3'\,|\,\hat{f}\,|\,\kappa'\rangle\langle\kappa''\bar{\kappa}''\,|\,\hat{\tau}_2\,|\,3'\bar{\kappa}'\rangle_{\tilde{S}}\right]\\&+\sum_{3'',4''}\langle 1''2''\,|\,\hat{v}\,|\,3''4''\rangle\langle 3''4''\,|\,\hat{t}_2\,|\,1'2'\rangle_{\tilde{S}}+\sum_{3',4'}\langle 3'4'\,|\,\hat{v}\,|\,1'2'\rangle\langle 1''2''\,|\,\hat{\tau}_2\,|\,3'4'\rangle_{\tilde{S}}\\&+\sum_{\kappa,\lambda=1}^{2}(-1)^{(\kappa+\lambda)\tilde{S}}\sum_{3'',3'}\sum_{S=0}^{1}\left[\tfrac{1}{2}([\tilde{S}][S])^{1/2}\langle\kappa''3'\,|\,\hat{v}\,|\,\bar{\lambda}'3''\rangle-\delta_{\tilde{S},S}\langle\kappa''3'\,|\,\hat{v}\,|\,3''\bar{\lambda}'\rangle\right]\langle 3''\bar{\kappa}''\,|\,\hat{\tau}_2\,|\,\lambda'3'\rangle_S\end{aligned} \tag{36}$$

and

$$\Lambda^{(2)}(1''2'',1'2';\tilde{S})\equiv\Lambda^{(2)}=\Lambda^{(2)}_{1,2}+\Lambda^{(2)}_3+\Lambda^{(2)}_4+\Lambda^{(2)}_5\ , \tag{37}$$

with

$$\Lambda^{(2)}_{1,2}=\tfrac{1}{4}[\tilde{S}]^{1/2}\sum_{\kappa=1}^{2}(-1)^{\kappa\tilde{S}}\sum_{S,S'=0}^{1}(-1)^{S+S'}([S][S'])^{1/2}\sum_{3',4',3'',4''}\{F(\tilde{S}+S+S')\langle 3'4'\,|\,\hat{v}\,|\,4''3''\rangle-\langle 3'4'\,|\,\hat{v}\,|\,3''4''\rangle\}\times\langle 1''3''\,|\,\hat{\tau}_2\,|\,\kappa'3'\rangle_S\langle 2''4''\,|\,\hat{\tau}_2\,|\,\bar{\kappa}'4'\rangle_{S'}\ , \tag{38a}$$

$$\Lambda^{(2)}_3=\tfrac{1}{2}\sum_{\kappa=1}^{2}(-1)^{\kappa\tilde{S}}\sum_{S=0}^{1}[S]^{1/2}\sum_{3',4',3'',4''}\langle 3'4'\,|\,\hat{v}\,|\,3''4''\rangle\langle 4''\kappa''\,|\,\hat{\tau}_2\,|\,1'2'\rangle_{\tilde{S}}\langle\bar{\kappa}''3''\,|\,\hat{\tau}_2\,|\,3'4'\rangle_S\ , \tag{38b}$$

$$\Lambda^{(2)}_4=\tfrac{1}{2}\sum_{\kappa=1}^{2}(-1)^{\kappa\tilde{S}}\sum_{S=0}^{1}[S]^{1/2}\sum_{3',4',3'',4''}\langle 3'4'\,|\,\hat{v}\,|\,3''4''\rangle\langle 1''2''\,|\,\hat{\tau}_2\,|\,\bar{\kappa}'4'\rangle_{\tilde{S}}\langle 3''4''\,|\,\hat{\tau}_2\,|\,\kappa'3'\rangle_S\ , \tag{38c}$$

$$\Lambda^{(2)}_5=(-1)^{1+\tilde{S}}\tfrac{1}{2}[\tilde{S}]^{-1/2}\sum_{3',4',3'',4''}\langle 3'4'\,|\,\hat{v}\,|\,3''4''\rangle\langle 1''2''\,|\,\hat{\tau}_2\,|\,3'4'\rangle_{\tilde{S}}\langle 3''4''\,|\,\hat{\tau}_2\,|\,1'2'\rangle_{\tilde{S}}\ , \tag{38d}$$

where

$$\bar{\kappa}=1+\delta_{1,\kappa},\quad \kappa=1,2\ \ (\text{i.e., }\bar{1}=2,\ \bar{2}=1) \tag{39}$$

and

$$-F(0)=F(1)=1,\quad F(2)=\tfrac{1}{3},\quad F(3)=\tfrac{5}{9}\ .$$

The nonlinear part $\Lambda^{(2)}$ has been broken down into the contributions from the individual diagrams as indicated by the subscript. Note also that the four terms $\Lambda^{(2)}_{1,2}$, $\Lambda^{(2)}_3$, $\Lambda^{(2)}_4$, and $\Lambda^{(2)}_5$ are associated with the four Hugenholtz diagrams arising from the disconnected tetraexcited cluster component $\frac{1}{2}\hat{T}^2_2$, shown in Fig. 5. Finally, projecting Eq. (8) onto the reference configuration $|\Phi_0\rangle$ we obtain the energy $\Delta\epsilon$ (Fig. 6),

$$\Delta\epsilon=\langle\Phi_0\,|\,\hat{H}_N\hat{T}_2\,|\,\Phi_0\rangle_C\ ,$$
$$=\tfrac{1}{2}\sum_{1',2',1'',2''}\langle 1'2'\,|\,\hat{v}\,|\,1''2''\rangle\sum_{S=0}^{1}(-1)^{1+S}[S]^{1/2}\times\langle 1''2''\,|\,\hat{\tau}_2\,|\,1'2'\rangle_S\ . \tag{40}$$

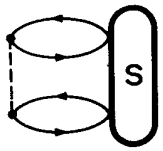

FIG. 6. The correlation energy resulting orbital diagram obtained by projecting Eq. (8) onto the reference state $|\Phi_0\rangle$ and yielding Eq. (40).

Assuming an arbitrary but fixed ordering for the $\hat{t}_2$ matrix elements (orthogonally spin adapted or not) and designating them simply by t_i $(i=1,\ldots,m)$, the nonlinear algebraic system of CC equations (32), which determines them, has the form

$$a_i+\sum_j b_{ij}t_j+\sum_{j\le k}c_{ijk}t_jt_k=0\ \ (i=1,\ldots,m)\ . \tag{41}$$

Setting $c_{ijk}=0$ we obtain the corresponding linear approximation (L-CCD). Finally, considering only diagrams 4 and 5 of Fig. 4 when calculating the nonlinear coefficients c_{ijk} (i.e., the terms $\Lambda^{(2)}_4$ and $\Lambda^{(2)}_5$) we obtain the ACP-D45 approximation.

III. APPROXIMATE ACCOUNT OF TETRAEXCITED CONNECTED CLUSTERS: MOTIVATION

Even though it would be quite feasible to work out the CC equations involving $\hat{T}_1$ through $\hat{T}_4$ components (for $\hat{T}_1$, $\hat{T}_2$, and $\hat{T}_3$ orthogonally spin-adapted formalism, see

Ref. 19) there is little hope that these equations could be solved in a foreseeable future for any realistic model. Indeed, it is sufficiently challenging to carry out such calculations involving the $\hat{T}_3$ as well as $\hat{T}_1$ and $\hat{T}_2$ components, so that one often resorts to approximating the $\hat{T}_3$ contribution only to a finite (fourth) order of perturbation theory (see, e.g., Ref. 8). Clearly, the principal source of complexity is the large number of equations, which increases with each excitation order by roughly the multiplicative factor $(n_h n_p)$, where n_h and n_p designate the number of hole and particle states, respectively. On the other hand, the required modification of the CCD equations which is brought about by the inclusion of either the $\hat{T}_3$ or $\hat{T}_4$ clusters is rather simple. Particularly in the latter case (for $\hat{T}_3$ see Refs. 16 and 19) we only have to consider one additional Hugenholtz diagram shown in Fig. 7. Consequently, if the $\hat{T}_4$ component, or its reasonable estimate, were available to us, it would be rather straightforward to include its contribution in the CCD equations. Since $\hat{T}_4$ is the highest cluster component which enters the CC(S)D equations, assuming pair interactions, these corrected equations (for both $\hat{T}_3$ and $\hat{T}_4$) would yield a very good correlation energy (in fact, we would get the exact result if exact $\hat{T}_3$ and $\hat{T}_4$ were used in solving the pair equations).

One could attempt, of course, to estimate the $\hat{T}_4$ components by the first few orders of the MBPT, similarly as it is currently done for the $\hat{T}_3$ contribution (cf. Ref. 8). However, since the first contribution will appear in the fifth order, this would be also computationally quite demanding. It would seem preferable, therefore, to estimate the $\hat{T}_4$ components and include them in pair equations via the diagram of Fig. 7. Considering the structure of the CC equations for quadruples, the main contribution can be expected to come via interaction of doubles through the diagrams of the type shown in Fig. 8. In view of the large number of quadruply excited components, one should in fact directly calculate the pertinent corrections to the CCD equations by substituting the diagrams of Fig. 8, approximating the $\hat{T}_4$ component, into the interaction term with the doubles, given by the diagram of Fig. 7. Thus, each CCD equation would be corrected by the diagrams shown in Fig. 9 (these yield 26 Hugenholtz diagrams when lines are oriented). Since each

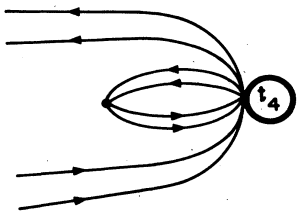

FIG. 7. Resulting Hugenholtz diagram containing one $\hat{T}_4$ vertex and obtained by projecting Eq. (8) onto the doubly excited state (22), $S_i \equiv \tilde{S}$. This diagram represents the contribution $\Lambda^{(3)}$, Eq. (34), to the CCD equations. In an ordinary CCD approach, this contribution is neglected.

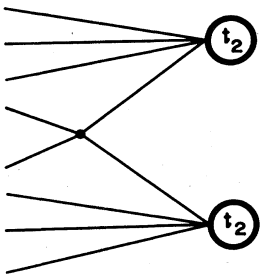

FIG. 8. A schematic Hugenholtz diagram representation of the nonlinear terms containing two T_2 vertices and contributing to the CC equations for quadruples, obtained by projecting Eq. (8) onto the quadruply excited states. This term can be expected to yield the most important contribution to the quadruply excited cluster manifold. Note that for the sake of simplicity we use nonoriented fermion lines, so that the above diagram represents in fact three diagrams which differ by the type of pair interaction: *pp*, *hh*, or *ph*.

such diagram involves six summations over the internal lines, four of which can be the particle lines, we are again facing quite a demanding computational task. (However, a similar approach to the $\hat{T}_3$ component, where only quadruple summations are involved, might be worth considering.) It is therefore worthwhile to look for the source of information about the T_4 clusters elsewhere.

As we mentioned earlier, the importance of the T_4 contribution increases with increasing quasidegeneracy of the reference state used. One of the very difficult cases is represented by the fully correlated limit of the cyclic polyene model (or, in fact, of any π-electron system), in which case all the one-electron contributions vanish, leading to a highly degenerate situation. The cluster analysis of the exact full CI wave functions for the first two cyclic polyenes ($N=6$ and 10) shows clearly the importance of the $\hat{T}_4$ component.[37] In fact, starting with $N=10$ there exist tetraexcited states which have no disconnected coun-

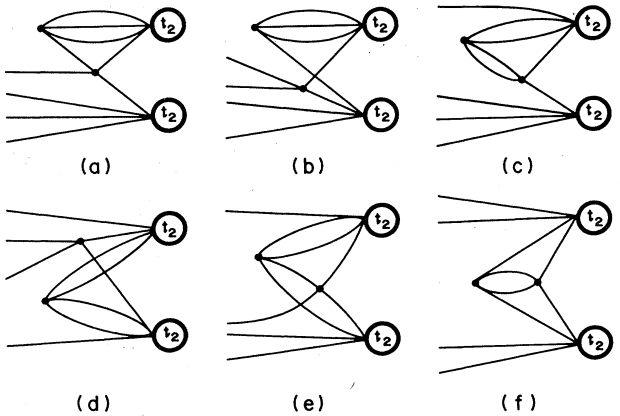

FIG. 9. A schematic Hugenholtz diagram representation of the lowest-order contribution of diagrams of Fig. 8 to pair cluster equations. Again, nonoriented fermion lines are used (see caption to Fig. 8) so that the six diagrams above represent in fact 26 Hugenholtz diagrams.

terpart and their number grows rapidly with N (i.e., for these states $\hat{C}_4=\hat{T}_4$). On the other hand, it is well known that the unrestricted Hartree-Fock (UHF) method of the DODS (different orbitals for different spins) type represents an excellent approximation for the large coupling constant regime (i.e., small resonance integral β values relative to the electron interaction integrals γ) and in fact provides the exact solution in the fully correlated limit (when $\beta=0$).[42] It is therefore tempting to exploit the UHF wave function to provide the information about the $\hat{T}_4$ cluster component.

It is also well known that the UHF reduces to the standard restricted Hartree-Fock (RHF) procedure whenever the latter is triplet (nonsinglet) stable.[43,44] Moreover, the transition between the stable and the unstable regions (separated by the critical value of the coupling constant) may show a nonanalytic behavior in either the density matrix or even the energy.[45] This transition may lead to various difficulties in both the CC and the MBPT approaches.[46,47] This behavior is of less concern for large or extended systems since the critical coupling constant becomes very small in such cases [e.g., for cyclic polyenes $|\beta_{\text{crit}}|\rightarrow\infty$ when $N\rightarrow\infty$, see Ref. 42(b)]. However, for finite molecular systems this behavior is of considerable concern.[46] It is thus preferable to exploit some projected procedure, such as the projected Hartree-Fock (PHF) method[48] or, if possible, the alternant molecular-orbital (AMO) method,[48–50] where the above-mentioned discontinuities are avoided. The AMO approach represents a special case of the PHF procedure (and is only applicable to minimum basis-set models) in which the restrictions on the coupling of occupied and virtual orbitals are so chosen that the most important correlation effects are well represented.

For the general development which we shall present below it is quite irrelevant which type of the broken-symmetry single determinantal solution is used and whether the optimization is carried out before (UHF) or after (PHF) projecting out the relevant symmetry component. We shall thus consider a general broken-symmetry (BS) single antisymmetrized product wave function of the form

$$|\Phi_{\text{BS}}\rangle=\exp(\hat{R}_1)\,|\Phi_0\rangle\ , \tag{42}$$

or its projected symmetry-adapted version $|\Phi\rangle=\hat{P}\,|\Phi_{\text{BS}}\rangle$ where $\hat{P}$ designates the pertinent symmetry projector. Thus, we can use either the UHF, PHF, or AMO wave functions or in fact any other broken-symmetry state (e.g., other types of UHF solutions as classified by Fukutome[51] or other broken-symmetry solutions, such as those found for singlet-unstable[43] RHF, etc.). The monoexcitation operator $\hat{R}_1$ for the spin-broken-symmetry cases (UHF, PHF, AMO) has the form

$$\hat{R}_1=\sum_{a^1,a_1}\langle a^1|\hat{r}_1|a_1\rangle\sum_{\sigma}(-1)^{1/2+\sigma}\hat{X}^{\dagger}_{a^1\sigma}\hat{X}_{a_1\sigma}\ , \tag{43}$$

namely, it consists of triplet monoexcitations with zero z component of spin $(\hat{X}^{\dagger}_{p\alpha}\hat{X}_{h\alpha}-\hat{X}^{\dagger}_{p\beta}\hat{X}_{h\beta})$. For the sake of brevity we shall designate its matrix elements as follows:

$$\langle a^1||a_1\rangle\equiv\langle 1''||1'\rangle:=\langle a^1|\hat{r}_1|a_1\rangle\ . \tag{44}$$

The diagrammatic representation of $\hat{R}_1$ is shown in Fig. 10(a), while the general multiple diagrams representing the multiply excited components of $|\Phi_{\text{BS}}\rangle$, Eq. (42), are illustrated by Figs. 10(b) and 10(c). Note that we represent the triplet coupled vertex by a one in a square and associate with it the matrix elements (44).

The resulting broken-symmetry wave function $|\Phi_{\text{BS}}\rangle$ with $\hat{R}_1$ defined by Eq. (43) contains various higher multiplets (triplets, quintets, etc.), which can be projected out obtaining a multideterminantal state $\hat{P}_{S=0}|\Phi_{\text{BS}}\rangle$. At this stage there is formally no difference between the UHF, PHF, or AMO procedures, since they will only differ in actual values of the matrix elements (44). In each case, these coefficients are determined from the variational principle which is applied before the projection in the UHF case and after the projection in the PHF and AMO cases. In the last case, a further restriction on the coefficients (44) is imposed by considering only the monoexcitations between the alternately conjugate pairs of orbitals.[50] In the following, we shall thus use the projected form of the UHF-type wave function in order to estimate the contribution of connected quadruply excited clusters.

IV. CORRECTIONS FOR QUADRUPLY EXCITED CONNECTED CLUSTERS

To correct the CCD equations for the $\hat{T}_4$ contribution as approximated by the projected broken-symmetry wave function $\hat{P}_0|\Phi_{\text{BS}}\rangle$, Eq. (42), we first express the latter in the exponential form

$$\hat{P}_0|\Phi_{\text{BS}}\rangle=\hat{P}_0\exp(\hat{R}_1)|\Phi_0\rangle=\exp(\hat{K})|\Phi_0\rangle\ , \tag{45}$$

where $\hat{P}_0$ designates the projector onto the singlet manifold. For the spin broken-symmetry wave function of the UHF, PHF, or AMO type considered, the operator $\hat{K}$ can contain only even-number-of-times-excited components, i.e.,

$$\hat{K}=\hat{K}_2+\hat{K}_4+\cdots\ , \tag{46}$$

since all odd-number-of-times-excited contributions will be annihilated by the singlet projector $\hat{P}_0$.

In order to determine first the pair operator $\hat{K}_2$ we

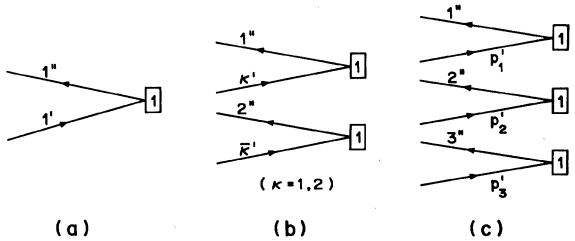

FIG. 10. Diagrammatic representation of (a) the monoexcitation operator $\hat{R}_1$, Eq. (43), and (b) and (c) of disconnected components arising through the exponential *Ansatz*, Eq. (42), representing multiply excited contributions. The triplet character of the monoexcitations is indicated by the rectangular vertex enclosing number 1 for $S=1$.

must examine the doubly excited component of $|\Phi_{BS}\rangle$ which arises by the action of the operator $\frac{1}{2}\hat{R}_1^2$,

$$\frac{1}{2}\hat{R}_1^2=\frac{1}{2}\sum_{1'',1'}\sum_{2'',2'}\langle 1''||1'\rangle\langle 2''||2'\rangle \times\sum_{\sigma,\tau}(-1)^{1+\sigma+\tau}\hat{X}^{\dagger}_{a^1\sigma}\hat{X}_{a_1\sigma}\hat{X}^{\dagger}_{a^2\tau}\hat{X}_{a_2\tau}\,. \tag{47}$$

This component is diagrammatically represented by Fig. 10(b), $\kappa=1$, with a^i, a_i $(i=1,2)$ being free labels.[15] For a fixed set of hole-particle labels, say a^1,a^2,a_1,a_2, both diagrams $\kappa=1$ and 2, Fig. 10(b), must be considered and the configurations associated with the products $\langle 1''||1'\rangle\langle 2''||2'\rangle$ and $\langle 1''||2'\rangle\langle 2''||1'\rangle$ are linearly independent (unless $a^1=a^2$ and/or $a_1=a_2$). We can thus express them in terms of single determinantal states (20) as follows:

$$\frac{1}{2}\hat{R}_1^2|\Phi_0\rangle=\frac{1}{2}\sum_{1'',2''}\sum_{1',2'}(\langle 1''||1'\rangle\langle 2''||2'\rangle|\Phi_{(+)}\rangle +\langle 1''||2'\rangle\langle 2''||1'\rangle|\Phi_{(-)}\rangle)\,, \tag{48}$$

where

$$|\Phi_{(+)}\rangle=\frac{1}{2}\sum_{\sigma,\tau}(-1)^{1+\sigma+\tau}\hat{X}^{\dagger}_{a^1\sigma}\hat{X}_{a_1\sigma}\hat{X}^{\dagger}_{a^2\tau}\hat{X}_{a_2\tau}|\Phi_0\rangle =\frac{1}{2}(G_1+G_2-G_3-G_4)\,, \tag{49}$$

$$|\Phi_{(-)}\rangle=\frac{1}{2}\sum_{\sigma,\tau}(-1)^{1+\sigma+\tau}\hat{X}^{\dagger}_{a^1\sigma}\hat{X}_{a_2\sigma}\hat{X}^{\dagger}_{a^2\tau}\hat{X}_{a_1\tau}|\Phi_0\rangle =\frac{1}{2}(-G_1-G_2+G_5+G_6)\,,$$

and ultimately in terms of the *pp-hh* coupled spin-adapted states (16) or (21), since

$$|\Phi_{(\pm)}\rangle=\tfrac{1}{2}|0\rangle_0^0\pm\tfrac{1}{2}(3)^{-1/2}|0\rangle_1^1\pm(\tfrac{2}{3})^{1/2}|2\rangle_1^1\,, \tag{50}$$

as may be easily found by calculating the overlaps between the states (49) and (21). Note that the states $|\Phi_{(\pm)}\rangle$, Eqs. (49), are contaminated by the quintet component but contain no triplet component. It should also be stressed that Eqs. (21) and (49) assume distinct hole-particle labels, i.e., $a^1\neq a^2$, $a_1\neq a_2$. Otherwise, the right-hand side of Eqs. (21) must be multiplied by the factor N_a, Eq. (19). Thus, we finally get

$$\hat{P}_0(\tfrac{1}{2}R_1^2)|\Phi_0\rangle=\frac{1}{4}\sum_{1'',2''}\sum_{1',2'}\{(\langle 1''||1'\rangle\langle 2''||2'\rangle+\langle 1''||2'\rangle\langle 2''||1'\rangle)|0\rangle_0^0 +(3)^{-1/2}(\langle 1''||1'\rangle\langle 2''||2'\rangle-\langle 1''||2'\rangle\langle 2''||1'\rangle)|0\rangle_1^1\}$$

$$=\frac{1}{4}\sum_{1'',2''}\sum_{1',2'}\sum_{S}[S]^{-1/2}(\langle 1''||1'\rangle\langle 2''||2'\rangle+(-1)^S\langle 1''||2'\rangle\langle 2''||1'\rangle)\left|\begin{matrix}1'' & 2''\\ 1' & 2'\end{matrix}\right\rangle_S N_a^{-1}\,, \tag{51}$$

where

$$\left|\begin{matrix}1'' & 2''\\ 1' & 2'\end{matrix}\right\rangle_S\equiv\left|\begin{matrix}a^1 & a^2\\ a_1 & a_2\end{matrix}\right\rangle_S$$

is defined by Eqs. (16) and (22).

Defining the orthogonally spin-adapted elements of the biexcited component $\hat{K}_2$ by analogy with the definition of $\hat{T}_2$ components, Eqs. (24) and (25), we get analogously to Eq. (26) that

$$(\hat{K}_2|\Phi_0\rangle)_{S=0}=\frac{1}{4}\sum_{S=0}^{1}\sum_{1'',2''}\sum_{1',2'}N_a^{-2}\langle 1''2''|\hat{k}_2|1'2'\rangle_S \times\left|\begin{matrix}1'' & 2''\\ 1' & 2'\end{matrix}\right\rangle_S\,, \tag{52}$$

so that

$$N_a^{-1}\langle 1''2''|\hat{k}_2|1'2'\rangle_S =[S]^{-1/2}\{\langle 1''||1'\rangle\langle 2''||2'\rangle +(-1)^S\langle 1''||2'\rangle\langle 2''||1'\rangle\}\,. \tag{53}$$

Using a nonorthogonally spin-adapted expression for $\hat{K}_2$ with matrix elements $\langle 1''2''|\hat{k}_2|1'2'\rangle$, we get by analogy with Eqs. (12), (29), (30), or (31) that

$$\langle 1''2''|\hat{k}_2|1'2'\rangle=\tfrac{1}{2}(-\langle 1''2''|\hat{\kappa}_2|1'2'\rangle_0 +3^{-1/2}\langle 1''2''|\hat{\kappa}_2|1'2'\rangle_1)\,, \tag{54}$$

where we defined the unnormalized $\hat{\kappa}_2$ elements by analogy with Eq. (28),

$$\langle 1''2''|\hat{\kappa}_2|1'2'\rangle_S=N_a^{-1}\langle 1''2''|\hat{k}_2|1'2'\rangle_S \qquad (S=0,1) \tag{55}$$

so that

$$\langle 1''2''|\hat{k}_2|1'2'\rangle=-\tfrac{1}{3}(\langle 1''||1'\rangle\langle 2''||2'\rangle +2\langle 1''||2'\rangle\langle 2''||1'\rangle)\,. \tag{56}$$

This last relationship can be also easily derived directly when we exploit the fact that the spin projector commutes with the Hamiltonian (or its two-particle components), which is assumed to be spin independent. This immediately implies the equality of energy contributions

$$\langle\Phi_0|\hat{V}_N\hat{K}_2|\Phi_0\rangle=\langle\Phi_0|\hat{V}(\tfrac{1}{2}\hat{R}_1^2)|\Phi_0\rangle\,. \tag{57}$$

In fact, the same procedure would apply to the projection

of any biexcitation formed from effective triplet coupled operators, so that we shall write

$$\Theta_d=\langle 1''2''\,|\,\hat{k}_2\,|\,1'2'\rangle,\quad \Theta_e=\langle 1''2''\,|\,\hat{k}_2\,|\,2'1'\rangle\ , \tag{58}$$

and

$$\Omega_d=\langle 1''||1'\rangle\langle 2''||2'\rangle,\quad \Omega_e=\langle 1''||2'\rangle\langle 2''||1'\rangle\ , \tag{59}$$

with the understanding that $\hat{\Theta}$ and $\hat{\Omega}$ can be any operators of the type $\hat{K}_2$ and $\hat{R}^2_1$, respectively. Representing these operators diagrammatically in the same way as the operators $\hat{K}_2$ and $\hat{R}_1$, we see immediately that the left- and right-hand members of Eq. (57) are given by the diagrams shown in Figs. 11(a) and 11(b), respectively. We find that any diagram which contains a closed loop of fermion lines with an odd number of triplet vertices gives a vanishing contribution [i.e., the first diagram of Fig. 11(b) in our case]. Thus, Eq. (57) implies that

$$2\Theta_d-\Theta_e=-\Omega_e\ . \tag{60}$$

Writing Θ_d as a linear combination of Ω's,

$$\Theta_d=a\Omega_d+b\Omega_e\ , \tag{61}$$

so that also

$$\Theta_e=a\Omega_e+b\Omega_d\ , \tag{61'}$$

we obtain by substituting into Eq. (60) that

$$2\Theta_d-\Theta_e=\Omega_d(2a-b)+\Omega_e(2b-a)=-\Omega_e\ . \tag{62}$$

Comparing the coefficients at the same terms we get a simple linear system for a and b coefficients,

$$\begin{aligned}2a-b&=0\ ,\\ 2b-a&=-1\ ,\end{aligned} \tag{63}$$

which has the solution

$$a=-\tfrac{1}{3},\quad b=-\tfrac{2}{3}\ . \tag{64}$$

We have thus recovered expression (56) and, in fact, obtained a simple rule for the projection of a product of triplet coupled excitations.

We are now ready to derive the corrections to the CCD equations due to the connected tetraexcited clusters. In order to estimate the $\hat{T}_4$ contribution, we must consider the tetraexcited component

$$\hat{P}_0\left[\frac{1}{4!}\hat{R}^4_1\right]|\,\Phi_0\rangle=(\tfrac{1}{2}\hat{K}^2_2+\hat{K}_4)\,|\,\Phi_0\rangle\equiv\hat{C}'_4\,|\,\Phi_0\rangle\ , \tag{65}$$

where the prime on $\hat{C}'_4$ indicates that this component is only an approximation to the exact tetraexcited component $\hat{C}_4$, Eq. (3). As we showed in the Sec. III, we are only interested in the evaluation of the coupling bi-tetraexcited terms as given by the diagram of Fig. 7, which will be used to correct the CCD Eqs. (32) by the term $\Lambda^{(3)}$, Eq. (34). This correction is thus given by

$$\begin{aligned}\Lambda^{(3)}&=\langle\Phi^{(2)}_i\,|\,\hat{V}_N\hat{K}_4\,|\,\Phi_0\rangle=\langle\Phi^{(2)}_i\,|\,\hat{V}_N(\hat{C}'_4-\tfrac{1}{2}\hat{K}^2_2)\,|\,\Phi_0\rangle\\ &\equiv\Lambda^{(3)}_4-\Lambda^{(3)}_{(2,2)}\ ,\end{aligned} \tag{66}$$

where we defined

$$\begin{aligned}\Lambda^{(3)}_4&=\langle\Phi^{(2)}_i\,|\,\hat{V}_N\hat{C}'_4\,|\,\Phi_0\rangle\ ,\\ \Lambda^{(3)}_{(2,2)}&=\langle\Phi^{(2)}_i\,|\,\hat{V}_N(\tfrac{1}{2}\hat{K}^2_2)\,|\,\Phi_0\rangle\ .\end{aligned} \tag{67}$$

It should be also noticed that the projection onto the singlet component, Eq. (65), will be automatically achieved when calculating matrix elements (67), since $|\,\Phi^{(2)}_i\rangle$ is a pure singlet state and the singlet projector $\hat{P}_0$ commutes with any part of our Hamiltonian in view of its spin independence. In evaluating the matrix elements we can

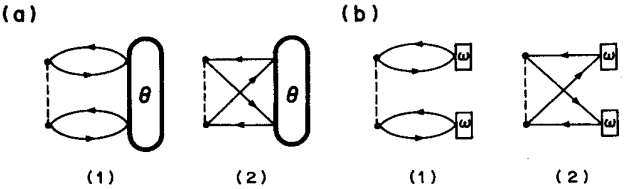

FIG. 11. Diagrammatic representation of the energy matrix elements given by (a) the left-hand member of Eq. (57) and (b) the right-hand member of Eq. (57). To stress the fact that the same relationship will hold for any pair operator $\hat{K}_2$ and triplet coupled monoexcitation-type operator $\hat{R}_1$, the corresponding vertices are labeled by θ and ω, respectively. Thus, for example, the ω vertex may represent any connected diagram containing an odd number of R_1 vertices and having only two external lines, while the θ vertex represents a standard singlet pair vertex.

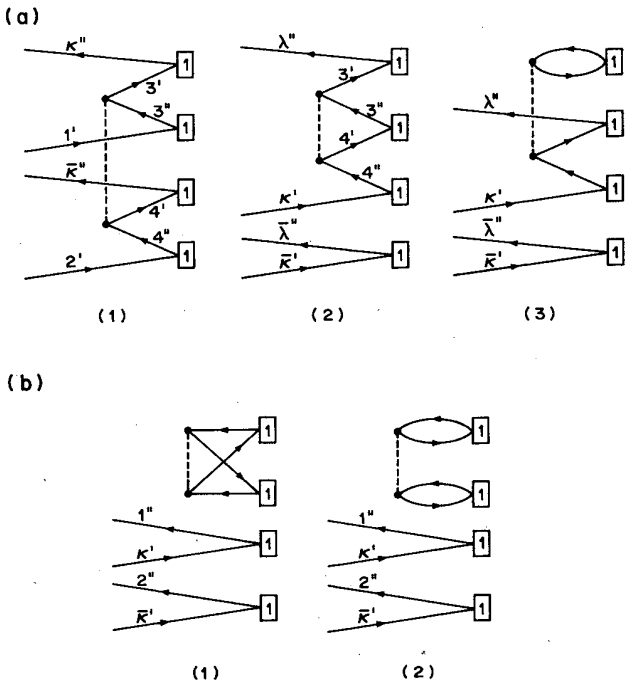

FIG. 12. The resulting Goldstone-type diagrams representing (a) the linked and (b) the unlinked contributions to $\Lambda^{(3)}_4$, Eq. (67). Diagram 3 of (a) and 2 of (b) give vanishing contributions.

distinguish linked and unlinked terms, even though we must exercise great care since in view of the approximation used we represent approximate connected clusters $\hat{K}_2$ or $\hat{K}_4$ through the products of triplet monoexcited clusters $\hat{R}_1$. We shall see, however, that considering both linked and unlinked clusters in evaluating $\Lambda^{(3)}$, the latter automatically disappear.

Let us rewrite Eq. (66) as

$$\Lambda^{(3)}=\Lambda_l^{(3)}+\Lambda_u^{(3)}=(\Lambda_4^{(3)}-\Lambda_{(2,2)}^{(3)})_l + (\Lambda_4^{(3)}-\Lambda_{(2,2)}^{(3)})_u \ , \tag{68}$$

where the subscript indicates the linked or unlinked character. The linked contributions to $\Lambda_4^{(3)}$, Eq. (67), are represented by the diagrams in Fig. 12(a) and the unlinked ones in Fig. 12(b). We have already seen that any closed loop of fermion lines which contains an odd number of triplet vertices makes the diagram vanish [i.e., the last diagram in Figs. 12(a) and 12(b)] so that only the first two diagrams of Fig. 12(a) and the first diagram of Fig. 12(b) have to be considered. In view of the formal similarity between the $\hat{K}_2$ and $\hat{T}_2$ operators, the linked diagrams (which are also connected) contributing to $\Lambda_{(2,2)}^{(3)}$ are identical with those of Fig. 4 (where, of course, we now associate the $\hat{k}_2$ or $\hat{\kappa}_2$ matrix elements with biexcited cluster vertices), while the unlinked contribution to $\Lambda_{(2,2)}^{(3)}$ is obtained by combining the diagrams in Figs. 1(a) and 6, yielding $\Delta\epsilon\langle a^1a^2\,|\,\hat{\kappa}_2\,|\,a_1a_2\rangle_{\tilde{S}}$. Using the energy expression, Eq. (40), and the representation of the $\hat{k}_2$ matrix elements, Eqs. (53) and (55), we easily find that the unlinked contributions in Eq. (68) cancel out so that we have

$$\Lambda^{(3)}=\Lambda_l^{(3)}=(\Lambda_4^{(3)}-\Lambda_{(2,2)}^{(3)})_l \ . \tag{69}$$

Expressing the CCD equations in the form (41) we can write the correction term $\Lambda^{(3)}$ as follows:

$$\Lambda^{(3)}=\tilde{a}_i-\sum_{j\le k}c_{ijk}k_jk_k \ , \tag{70}$$

where $\tilde{a}_i$ is given by the first two diagrams of Fig. 12(a) and k_j's label the $\hat{\kappa}_2$ matrix elements, which are assumed to be ordered in the same way as the corresponding $\hat{\tau}_2$ matrix elements so that the coefficients c_{ijk}, given by Eqs. (37)—(39), are identical in both cases. Thus, the modified CCD equations (which we could call CCDQ′ equations) including the approximate $\hat{T}_4$ contribution have the form

$$a_i+\tilde{a}_i+\sum_j b_{ij}t_j+\sum_{j\le k}c_{ijk}(t_jt_k-k_jk_k)=0 \ . \tag{71}$$

The matrix elements $k_i\equiv\langle a^1a^2\,|\,\hat{\kappa}_2\,|\,a_1a_2\rangle_S$ can be calculated from Eq. (53) once the monoexcited coefficients $\langle a^1\,|\,|\,a_1\rangle$, defining the UHF, PHF, or AMO wave function employed, are available. It thus remains to evaluate the contribution $\tilde{a}_i$ from the diagrams of Fig. 12(a). This can be most easily achieved via the nonorthogonally adapted formalism. Designating by $\lambda_j(a^\lambda a_\kappa;a^{\bar{\lambda}}a_{\bar{\kappa}})$ the unprojected contribution from the jth diagram of Fig. 12(a), $j=1,2$ (recall that $\lambda_3=0$ and note that arguments label the external lines associated with the two oriented paths in the standard way), the contributions to the two possible CCD equations, labeled by the fixed (distinct) particle labels a^1,a^2 and hole labels a_1,a_2, before the spin projection are [cf. notation of Eqs. (59) and (60) of Ref. 5]

$$\begin{aligned}\lambda_j^{(1)}&=\lambda_j(1''1';2''2')+\lambda_j(2''2';1''1') \ ,\\ \lambda_j^{(2)}&=\lambda_j(1''2';2''1')+\lambda_j(2''1';1''2') \ .\end{aligned} \tag{72}$$

Explicit expressions for these quantities follow easily from the diagrams of Fig. 12(a), namely

$$\lambda_1^{(\kappa)}=\sum_{3',4',3'',4''}\langle 3'4'\,|\,\hat{v}\,|\,3''4''\rangle\langle\kappa''||3'\rangle\langle\bar{\kappa}''||4'\rangle \times\langle 3''||1'\rangle\langle 4''||2'\rangle \ , \tag{73a}$$

$$\lambda_2^{(\kappa)}=\sum_{3',4',3'',4''}\langle 3'4'\,|\,\hat{v}\,|\,3''4''\rangle\langle 3''||4'\rangle \times(\langle 1''||3'\rangle\langle 4''||\kappa'\rangle\langle 2''||\bar{\kappa}'\rangle + \langle 2''||3'\rangle\langle 4''||\bar{\kappa}'\rangle\langle 1''||\kappa'\rangle) \ . \tag{73b}$$

To obtain spin projected contributions, we note that the resulting monoexcitations in the first diagram of Fig. 12(a) have a singlet character, so that they give directly the required contribution $\tilde{\lambda}_1$ to $\tilde{a}_i$ in the nonorthogonally spin-adapted (spin-bonded function) basis, namely

$$\begin{aligned}\tilde{\lambda}_1(d)&\equiv\tilde{\lambda}_1(1''2'';1'2')=\lambda_1^{(1)} \ ,\\ \tilde{\lambda}_1(e)&\equiv\tilde{\lambda}_1(1''2'';2'1')=\lambda_1^{(2)} \ .\end{aligned} \tag{74}$$

In the second diagram of Fig. 12(a) the two oriented paths represent triplet excitations so that we have to carry out the appropriate projection. This is simply achieved using the above outlined prescription [Eqs. (57)—(64)] so that

$$\begin{aligned}\tilde{\lambda}_2(d)&\equiv\tilde{\lambda}_2(1''2'';1'2')=-\tfrac{1}{3}(\lambda_2^{(1)}+2\lambda_2^{(2)}) \ ,\\ \tilde{\lambda}_2(e)&\equiv\tilde{\lambda}_2(1''2'';2'1')=-\tfrac{1}{3}(\lambda_2^{(2)}+2\lambda_2^{(1)}) \ .\end{aligned} \tag{75}$$

It is now straightforward to find the corresponding contributions in the orthogonally spin-adapted basis by applying the inverse transformation of Eq. (54) which gives

$$\begin{aligned}\Lambda_{4,j}^{(3)}&\equiv\Lambda_{4,j}^{(3)}(1''2'',1'2';\tilde{S})\\ &=-[\tilde{S}]^{1/2}\{(-1)^{\tilde{S}}\tilde{\lambda}_j(d)+\tilde{\lambda}_j(e)\} \ ,\end{aligned} \tag{76}$$

so that finally

$$\tilde{a}_j\equiv(\Lambda_4^{(3)})_l=\Lambda_{4,1}^{(3)}+\Lambda_{4,2}^{(3)} \ . \tag{77}$$

Explicitly

$$\Lambda_{4,1}^{(3)}(1''2'',1'2';\tilde{S})=-[\tilde{S}]^{1/2}\sum_{3',4',3'',4''}\{(-1)^{\tilde{S}}\langle 3'4'\,|\,\hat{v}\,|\,3''4''\rangle+\langle 3'4'\,|\,\hat{v}\,|\,4''3''\rangle\} \times\langle 1''||3'\rangle\langle 2''||4'\rangle\langle 3''||1'\rangle\langle 4''||2'\rangle \ , \tag{78a}$$

and

$$\Lambda^{(3)}_{4,2}(1''2'',1'2';\tilde{S})=[\tilde{S}]^{-1/2}[\lambda^{(1)}_2+(-1)^{\tilde{S}}\lambda^{(2)}_2]$$

$$=[\tilde{S}]^{-1/2}\sum_{3',4',3'',4''}\langle 3'4'\,|\,\hat{v}\,|\,3''4''\rangle\langle 3''||4'\rangle\sum_{\kappa,\lambda=1}^{2}(-1)^{(\kappa+\lambda)\tilde{S}}\langle\lambda''||3'\rangle\langle 4''||\kappa'\rangle\langle\bar{\lambda}''||\bar{\kappa}'\rangle\ . \tag{78b}$$

This completes the derivation of the explicit form of the CCDQ' Eqs. (71).

V. DISCUSSION

Assume for the moment that the projected state $\hat{P}_0\,|\,\Phi_{\rm BS}\rangle$, Eq. (45), is exact and that

$$t_j=k_j\ . \tag{79}$$

In this case Eqs. (71) reduce to the linear form

$$a_i+\tilde{a}_i+\sum_j b_{ij}t_j=0\ , \tag{80}$$

where $\tilde{a}_i$ are given by the first two diagrams of Fig. 12(a). Keeping in mind the relationship between the pair clusters, Eq. (79), and monoexcited triplet clusters, Eq. (44), as expressed by Eq. (53), we can examine which types of nonlinear diagrams of Fig. 4 or 5 are represented by the correction $\tilde{a}_i$ in CCDQ' Eqs. (80) under the assumption of Eq. (79). In order to see this correspondence we can make the replacement indicated in Fig. 13 which can be regarded as a diagrammatic representation of Eq. (53). This replacement is most easily implemented by considering the Goldstone form of nonlinear CCD diagrams of Fig. 4 or 5 (see Fig. 8 of Ref. 6), in which case it suffices to erase the nonoriented connecting lines as shown in Fig. 13(b). The resulting set of diagrams is shown in Fig. 14. We see that this operation yields the diagrams of Fig. 12: the unlinked diagrams of Fig. 12(b) occur once while each linked diagram of Fig. 12(a) is generated three times. On first sight it would seem that the effect of inclusion of the connected quadruply excited clusters $\hat{T}_4$, under the assumption of Eq. (79), can be regarded to be equivalent to deleting the first three nonlinear diagrams of Fig. 4 (or the first two Hugenholtz diagrams of Fig. 5) while keeping only the last two diagrams of Fig. 4 or 5, whose contribution is equivalent to the term $\tilde{a}_i$ of Eq. (80). With this interpretation, the CCDQ' Eqs. (80) would be exactly equivalent to the ACP-D45 approximation of the CCD equations discussed in the Introduction. We shall show shortly that while this interpretation is basically correct, it needs nevertheless some "fine tuning" (namely, the change of an integer factor of one of the diagram contribution). Before finding out this precise correspondence let us discuss the correspondence between $\tilde{a}_i$ diagrams and nonlinear CCD diagrams in more detail.

Since each diagram of Fig. 12(a) occurs three times among those of Fig. 14 one could of course devise other interpretations of the term $\tilde{a}_i$ in Eq. (80) than that given

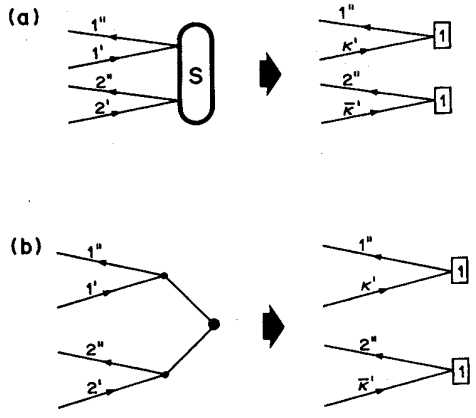

FIG. 13. A schematic diagrammatic representation of the relationship (53) between the pair K_2 clusters and R^2_1 clusters, and (b) corresponding relationship between standard pair and R^2_1 clusters as given by Eq. (56).

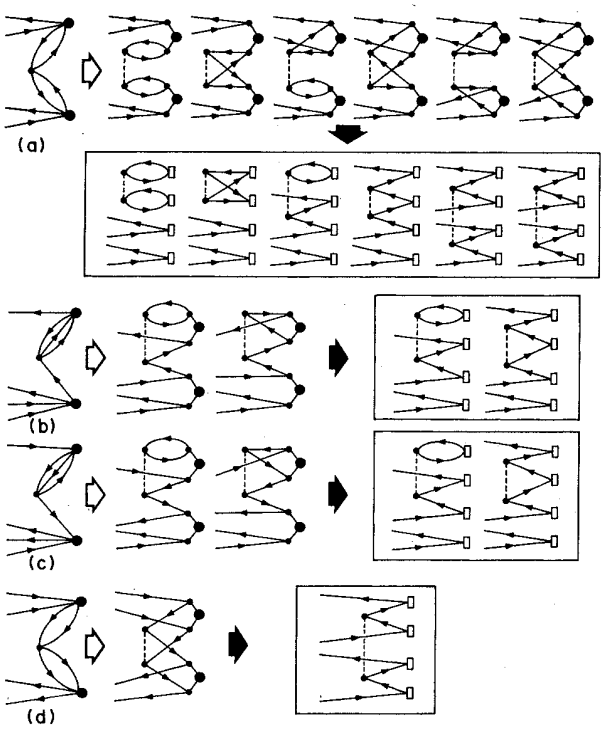

FIG. 14. A schematic representation of the relationship between the nonlinear CCD diagrams of Figs. 4 or 5, represented in the Hugenholtz form by diagrams (a)—(d), Fig. 4, and corresponding linked quadruple contributions, represented by diagrams of Fig. 12, as implied by the relationships (53) or (56) (see Fig. 13). For each Hugenholtz diagram (a)—(d) of Fig. 4 we first list the corresponding Goldstone versions (white arrow) followed by the application of the relationships (53) or (56), represented by the black arrow. The resulting diagrams of Fig. 12, approximating the quadruply excited cluster contribution to the CCD equations, are enclosed in rectangles.

above in terms of the ACP-D45 approximation. Even when we exclude the first two diagrams of Fig. 4 (i.e., the first Hugenholtz diagram of Fig. 5), since its counterparts in Fig. 14 contain unlinked diagrams of Fig. 12(b), we see that from the viewpoint of the comparison we are undertaking, diagrams 3 and 4 of Fig. 4 (or diagrams *b* and *c* of Fig. 5) play exactly the same role. In fact, these diagrams are closely related since they can be transformed one into the other by the hole-particle conjugation operation which reverses the orientation of each fermion line. In any system possessing the hole-particle symmetry, for example in alternant π-electron systems described by the semiempirical PPP (Pariser-Parr-Pople) Hamiltonian where the the Coulson-Rushbrooke pairing theorem holds, these diagrams will give exactly the same contribution, so that in fact the D45 approximation will be equivalent to the D35 approximation in such systems. Generally, however, the particle-hole symmetry is not present, in particular for *ab initio* model Hamiltonians when larger than the minimum basis set is used. Thus, while the above outlined correspondence (cf. Fig. 14) shows the ACP-D45 approximation in the new light, it does not unambiguously imply this approximation. In fact, the main reason for choosing the D45 approximation stems from the fact that these two diagrams give the EPV terms, which are proportional to the (occupied) pair energies, as discussed in more detail in Refs. 26 and 27. Indeed, in various CEPA-type approaches, only these EPV terms are retained. Another way of expressing this fact is to state that diagrams 4 and 5 of Fig. 4 factorize with respect to the pair energy contributions.

Let us, finally, carry out the detailed comparison between the CCDQ′ approximation via Eqs. (80) and the ACP-D45 approximation to the CCD equations. We can simply consider the terms originating from diagrams 4 and 5 of Fig. 4, as given by Eqs. (38c) and (38d), respectively, and use the relationship between the $\hat{k}_2$ and $\hat{r}_1$ matrix elements, Eq. (53), assuming Eq. (79) holds. From the contribution of diagram 4, Eq. (38c), we recover in this way precisely the contribution of the second diagram of Fig. 12(a) as given by Eq. (78b). [Recall that the last diagram of Fig. 12(a) gives a vanishing contribution.] However, from the contribution of diagram 5, Eq. (38d), we find that

$$\Lambda_5^{(2)}=[\tilde{S}]^{-3/2}\sum_{3',4',3'',4''}\{(-1)^{1+\tilde{S}}\langle 3'4'\,|\,\hat{v}\,|\,3''4''\rangle-\langle 3'4'\,|\,\hat{v}\,|\,4''3''\rangle\}\langle 1''||3'\rangle\langle 2''||4'\rangle\langle 3''||1'\rangle\langle 4''||2'\rangle$$

$$=[\tilde{S}]^{-2}\Lambda_{4,1}^{(3)}\,, \tag{81}$$

with $\Lambda_{4,1}^{(3)}$ given by Eq. (78a). Thus, while in the singlet equation ($\tilde{S}=0$) the contribution of the first diagram is again identical with that of diagram 5, Fig. 4, these contributions differ by the factor of 9 for the triplet ($\tilde{S}=1$) equation. Thus, assuming that Eq. (79) holds, which is equivalent to assuming that our UHF, PHF, or AMO wave function provides us with exact pair clusters, we find that the CCDQ′ equations, which reduce in this case to a simple form, Eq. (80), are identical with the ACP-D45 equations [provided the relationship (53) is employed] except for those which were obtained by projecting onto the biexcited configurations with triplet intermediate coupling of hole and particle pairs ($\tilde{S}=1$), in which case we have to multiply the fifth diagram contribution by the factor of 9. In order to distinguish this new approximation from the ACP-D45 (or simply ACP) approximation, we refer to it as the ACP-D45(9_3) or simply as the ACPQ (approximate coupled pairs with quadruples) approach. Needless to say that the simple relationship between the ACPQ and ACP approaches (a factor of 9 for the fifth nonlinear diagram in triplet coupled equations) can only be achieved when we employ the *orthogonally* spin-adapted formalism.[18]

To regard the ACPQ equations from yet another angle, we can also make a similar comparison between the linear part of the CCD equations, Eq. (36), and the corresponding terms, which arise when we consider the projected UHF-type wave function in lieu of the cluster *Ansatz* in the Schrödinger equation (8). Projecting onto the biexcited configurations $|\Phi_i^{(2)}\rangle$ as in Eqs. (32)–(34), we obtain the system

$$\langle\Phi_i^{(2)}\,|\,\hat{H}_N\hat{P}_0e^{\hat{R}_1}\,|\,\Phi_0\rangle=\langle\Phi_i^{(2)}\,|\,\hat{H}_Ne^{\hat{R}_1}\,|\,\Phi_0\rangle=0\,. \tag{82}$$

This yields $\sim(nm)^2$ equations for only $\sim(nm)$ variables $\langle a^1\,|\,\hat{r}_1\,|\,a_1\rangle$. However, making the replacements of the products of $\hat{r}_1$ matrix elements by pair clusters, following the relationship given by Eq. (53), or rather its inverse, Eq. (A15), we can restore the correct number of independent unknowns. This removes the restrictions placed on the higher-excited components by the structure of the UHF wave function. In this way we also find a complete correspondence between all the bilinear terms in the $\hat{r}_1$ matrix elements and the linear terms of the CCD equations as shown in the Appendix. We recall that for the quadruply excited part this complete correspondence was only found for diagram 4 of Fig. 4, while for diagram 5 of Fig. 4 an extra factor of 9 was introduced. Consequently, we can also regard the ACPQ equations as arising from the PHF-type equations (82) by replacing the products of R_1 matrix elements by the $\hat{t}_2$ (or $\hat{k}_2$) matrix elements according to the rule expressed by Eq. (53), or Eq. (A15).

Let us mention, finally, that it would be very desirable to handle the effect of triexcited clusters $\hat{T}_3$ in a manner similar to the way we handled the $\hat{T}_4$ clusters in this paper. Of course, this is not possible using the UHF-, PHF-, or AMO-type wave function exploited here since no triexcited singlets can be projected from the wave function of the type given by Eqs. (42) and (43). However, this might be possible when using other types of broken-symmetry wave function to estimate $\hat{T}_3$ component.

VI. CONCLUSIONS

The consideration of the connected tetraexcited cluster components $\hat{T}_4$ is important whenever the reference state $|\Phi_0\rangle$ becomes quasidegenerate and is absolutely essential in extended metalliclike systems, such as linear polyenic chains. It is well known that the inclusion of these clusters represents a very formidable task. We have shown in this paper that the effect of these clusters can be taken into account in a surprisingly simple way by a slight modification of the approximate coupled-pair theory suggested and exploited earlier.[26–28] This fact also explains the successes of the ACP and the fact that whenever applied in cases where exact solution was available from the full CI treatment, the ACP provided better results than the full CCD or CCSD approaches. We will show in forthcoming papers how this approach is essential for handling of metalliclike systems mentioned above. In fact, these papers will show that while the usual CC(S)D approach breaks down altogether for sufficiently large cyclic polyenes, the ACPQ approach provides the exact solution in the fully correlated limit, while having practically no effect in the weakly correlated limit. Thus, this approach yields very good results in the whole range of the coupling constant. This paper also explains why even cruder approximations, such as various CEPA-type approaches, can provide relatively good results in nondegenerate as well as quasidegenerate situations.

ACKNOWLEDGEMENTS

This work was supported by Natural Sciences and Engineering Research Council of Canada Grants-in-Aid of Research (J.P. and J.C.) which are hereby gratefully acknowledged. One of the authors (M.T.) would like to express his thanks to the Department of Applied Mathematics of the University of Waterloo, and in particular to his coauthors for their hospitality during his stay as a Postdoctoral Fellow.

APPENDIX

We shall establish a detailed relationship between the bilinear part of Eqs. (82) and the linear part of the CCD equations (32). In other words, we wish to inter-relate the second-order triplet cluster terms, projected onto the biexcited states, $\langle\Phi_i^{(2)}|\hat{H}_N(\frac{1}{2}\hat{R}_1^2)|\Phi_0\rangle$, and the linear pair cluster terms of the CCD approach, $\langle\Phi_i^{(2)}|\hat{H}_N\hat{T}_2|\Phi_0\rangle$. The relationship between corresponding projections onto the reference state $|\Phi_0\rangle$, Eq. (57), which provided us with a simple rule for the projection of products of triplet coupled components, was given in Sec. IV, Eqs. (57)–(64).

The resulting Goldstone diagrams, which represent the matrix element $\langle\Phi_i^{(2)}|\hat{H}_N(\frac{1}{2}\hat{R}_1^2)|\Phi_0\rangle$ and consist of two triplet-type monoexcitation vertices [Fig. 10(a)] and one interaction (one- or two-particle) vertex are given in Fig. 15. We can easily associate them with the diagrams of Fig. 3 which give rise to the linear CCD terms: diagram 1 (2) in which a particle (hole) is scattered by the one-particle term of $\hat{H}_N$ corresponds to diagram 1_p (1_h) of Fig. 3, diagram 3 (4) with a particle-particle (hole-hole) ladder-type interaction corresponds to diagram 2_p (2_h) of Fig. 3 and, finally, diagrams 5–8 [diagram 8 vanishes for the same reason as diagram 3 of Fig. 12(a) and 2 of Fig. 12(b)] involving the hole-particle ladder- and ring-type interactions correspond to the diagrams 2_{ph} and $2'_{ph}$ of Fig. 3.

Using an analogous notation to that employed on the right-hand side of Eq. (72), we designate the contribution from the ith diagram of Fig. 15, whose external lines of the two distinct paths carry the labels κ'',λ' and $\bar{\kappa}'',\bar{\lambda}'$ (where $\bar{x}=1+\delta_{1x}$, $x=\kappa,\lambda$), by $\mu_i\equiv\mu_i(\kappa''\lambda';\bar{\kappa}''\bar{\lambda}')$. The explicit algebraic form of these contributions is found easily (we assume all labels to be free[15]) from the diagrams of Fig. 15, namely,

$$\mu_1=\sum_{3''}\langle\kappa''|\hat{f}|3''\rangle\langle 3''||\lambda'\rangle\langle\bar{\kappa}''||\bar{\lambda}'\rangle\ , \tag{A1}$$

$$\mu_2=-\sum_{3'}\langle 3'|\hat{f}|\lambda'\rangle\langle\kappa''||3'\rangle\langle\bar{\kappa}''||\bar{\lambda}'\rangle\ , \tag{A2}$$

$$\mu_3=\tfrac{1}{2}\sum_{3'',4''}\langle\kappa''\bar{\kappa}''|\hat{v}|3''4''\rangle\langle 3''||\lambda'\rangle\langle 4''||\bar{\lambda}'\rangle\ , \tag{A3}$$

$$\mu_4=\tfrac{1}{2}\sum_{3',4'}\langle 3'4'|\hat{v}|\lambda'\bar{\lambda}'\rangle\langle\kappa''||3'\rangle\langle\bar{\kappa}''||4'\rangle\ , \tag{A4}$$

$$\mu_5+\mu_6=-\sum_{3',3''}(\langle\bar{\kappa}''3'|\hat{v}|3''\lambda'\rangle\langle\kappa''||3'\rangle\langle 3''||\bar{\lambda}'\rangle + \langle\kappa''3'|\hat{v}|3''\lambda'\rangle \times\langle 3''||3'\rangle\langle\bar{\kappa}''||\bar{\lambda}'\rangle)\ , \tag{A5}$$

$$\mu_7=-\sum_{3',3''}\langle\bar{\kappa}''3'|\hat{v}|\bar{\lambda}'3''\rangle\langle\kappa''||3'\rangle\langle 3''||\lambda'\rangle\ , \tag{A6}$$

$$\mu_8=0\ . \tag{A7}$$

Now, except for diagram 7 (Fig. 15), whose oriented paths involve an even number of triplet monoexcitation vertices, we have to project out the singlet component. This can be achieved in the same way as outlined in Sec. IV. Combining relationships (72), (75), and (76) we obtain that

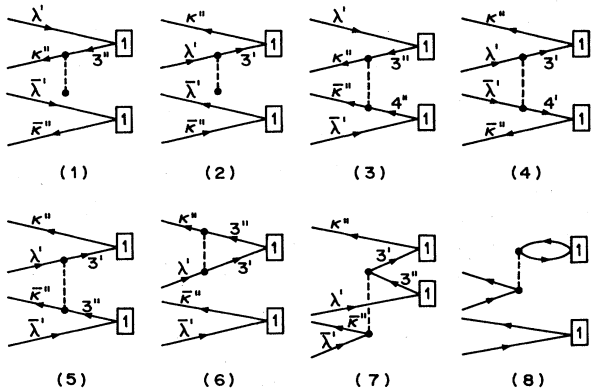

FIG. 15. The Goldstone-type diagrams representing the doubly excited contribution to Eq. (82). The same diagrams are also obtained by applying the transformation represented in Fig. 13 to the linear CCD diagrams of Fig. 3.

$$\Lambda_j(1''2'',1'2';\tilde{S}) = \tfrac{1}{3}[\tilde{S}]^{1/2}[2+(-1)^{\tilde{S}}] \times \sum_{\kappa,\lambda=1}^{2}(-1)^{(\kappa+\lambda)\tilde{S}}\lambda_j(\kappa''\lambda';\bar{\kappa}''\bar{\lambda}') = [\tilde{S}]^{-1/2}\sum_{\kappa,\lambda=1}^{2}(-1)^{(\kappa+\lambda)\tilde{S}}\lambda_j(\kappa''\lambda';\bar{\kappa}''\bar{\lambda}') . \quad \text{(A8)}$$

Thus, replacing λ's with μ's and designating analogously the contribution of the ith diagram of Fig. 15 projected onto the biexcited state

$$\left|\begin{matrix}1'' & 2''\\ 1' & 2'\end{matrix}\right\rangle_{\tilde{S}}$$

by $M_j \equiv M_j(1''2'',1'2';\tilde{S})$ we get

$$M_1=[\tilde{S}]^{-1/2}\sum_{\kappa,\lambda=1}^{2}(-1)^{(\kappa+\lambda)\tilde{S}}\sum_{3''}\langle\kappa''|\hat{f}|3''\rangle\langle 3''||\lambda'\rangle\langle\bar{\kappa}''||\bar{\lambda}'\rangle , \quad \text{(A9)}$$

$$M_2=-[\tilde{S}]^{-1/2}\sum_{\kappa,\lambda=1}^{2}(-1)^{(\kappa+\lambda)\tilde{S}}\sum_{3'}\langle 3'|\hat{f}|\lambda'\rangle\langle\kappa''||3'\rangle\langle\bar{\kappa}''||\bar{\lambda}'\rangle , \quad \text{(A10)}$$

$$M_3=[\tilde{S}]^{-1/2}\sum_{3'',4''}\langle 1''2''|\hat{v}|3''4''\rangle\sum_{\kappa=1}^{2}(-1)^{\bar{\kappa}\tilde{S}}\langle 3''||\kappa'\rangle\langle 4''||\bar{\kappa}'\rangle , \quad \text{(A11)}$$

$$M_4=[\tilde{S}]^{-1/2}\sum_{3',4'}\langle 3'4'|\hat{v}|1'2'\rangle\sum_{\kappa=1}^{2}(-1)^{\bar{\kappa}\tilde{S}}\langle\kappa''||3'\rangle\langle\bar{\kappa}''||4'\rangle , \quad \text{(A12)}$$

$$M_5+M_6=-[\tilde{S}]^{-1/2}\sum_{\kappa,\lambda=1}^{2}(-1)^{(\kappa+\lambda)\tilde{S}}\sum_{3',3''}\langle\kappa''3'|\hat{v}|3''\bar{\lambda}'\rangle\{\langle\bar{\kappa}''||3'\rangle\langle 3''||\lambda'\rangle+(-1)^{\tilde{S}}\langle 3''||3'\rangle\langle\bar{\kappa}''||\lambda'\rangle\} . \quad \text{(A13)}$$

For diagram 7 (Fig. 15) we only have to apply the transformation analogous to that of Eq. (76) since in this case Eq. (74) holds, so that

$$M_7=[\tilde{S}]^{1/2}\sum_{\kappa,\lambda=1}^{2}(-1)^{(\kappa+\lambda)\tilde{S}}\sum_{3',3''}\langle\kappa''3'|\hat{v}|\bar{\lambda}'3''\rangle\langle\bar{\kappa}''||3'\rangle\langle 3''||\lambda'\rangle . \quad \text{(A14)}$$

We shall finally inter-relate the spin-adapted contributions of the diagrams in Fig. 15, Eqs. (A9)—(A14), with those originating from the linear CCD diagrams of Fig. 3. This can be achieved by replacing the products of $\hat{r}_1$ matrix elements by the corresponding pair clusters using the relationship of Eq. (53). Inverting this relationship we obtain

$$\langle 1''||1'\rangle\langle 2''||2'\rangle=\tfrac{1}{2}\sum_{S=0}^{1}[S]^{1/2}\langle 1''2''|\hat{\kappa}_2|1'2'\rangle_S . \quad \text{(A15)}$$

Replacing now the products of $\hat{r}_1$ matrix elements by the pair cluster elements using this last relationship we obtain the desired expressions. For example, for the first diagram contribution, Eq. (A9), we get

$$\begin{aligned}M_1(1''2'',1'2';\tilde{S}) &= [\tilde{S}]^{-1/2}\sum_{\kappa,\lambda=1}^{2}(-1)^{(\kappa+\lambda)\tilde{S}}\sum_{3''}\sum_{S=0}^{1}[S]^{1/2}\langle\kappa''|\hat{f}|3''\rangle\langle 3''\bar{\kappa}''|\hat{\kappa}_2|\lambda'\bar{\lambda}'\rangle_S\\ &= [\tilde{S}]^{-1/2}\sum_{\kappa=1}^{2}\sum_{3''}\sum_{S=0}^{1}(-1)^{\kappa\tilde{S}}[S]^{1/2}\langle\kappa''|\hat{f}|3''\rangle\{(-1)^{\tilde{S}}+(-1)^{S}\}\langle 3''\bar{\kappa}''|\hat{\kappa}_2|1'2'\rangle_S\\ &= [\tilde{S}]^{-1/2}\sum_{\kappa=1}^{2}\sum_{3''}\sum_{S=0}^{1}(-1)^{(\kappa+1)\tilde{S}}\delta_{S\tilde{S}}[S]^{1/2}\langle\kappa''|\hat{f}|3''\rangle\langle 3''\bar{\kappa}''|\hat{\kappa}_2|1'2'\rangle_S\\ &= \sum_{\kappa=1}^{2}\sum_{3''}\langle\kappa''|\hat{f}|3''\rangle\langle 3''\bar{\kappa}''|\hat{\kappa}_2|\kappa'\bar{\kappa}'\rangle_{\tilde{S}} . \end{aligned} \quad \text{(A16)}$$

The resulting expression is easily identified with the first term in $\Lambda^{(1)}$, Eq. (36), if we identify the $\hat{\kappa}_2$ and $\hat{\tau}_2$ matrix elements. In the same way, we find a similar correspondence for the remaining diagrams of Fig. 15, Eqs. (A10)—(A14), yielding eventually the whole $\Lambda^{(1)}$ contribution, Eq. (36). This completes the derivation of the desired correspondence.

*Also at: Department of Chemistry and Guelph-Waterloo Center for Graduate Work in Chemistry, Waterloo Campus, University of Waterloo.

†Also at: The Laboratory of the National Foundation for Cancer Research, Faculty of Mathematics, University of Waterloo.

[1]J. Hubbard, Proc. R. Soc. London, Ser. A **240**, 539 (1957); **243**, 336 (1958); **244**, 199 (1958).

[2]F. Coester, Nucl. Phys. **7**, 421 (1958); F. Coester and H. Kümmel, *ibid.* **17**, 477 (1960); H. Kümmel, in *Lectures on the Many-Body Problems,* edited by E. R. Caianiello (Academic, New York, 1962), p. 265.

[3]H. Primas, in *Modern Quantum Chemistry,* edited by O. Sinanoğlu (Academic, New York, 1965), Vol. 2, p. 45.
[4]Cf., e.g., W. D. Laidig, G. D. Purvis, and R. J. Bartlett, Int. J. Quantum Chem., Symp. **16**, 561 (1982); Chem. Phys. Lett. **97**, 209 (1983).
[5]J. Čížek, J. Chem. Phys. **45**, 4256 (1966).
[6]J. Čížek, Adv. Chem. Phys. **14**, 35 (1969).
[7]J. Čížek and J. Paldus, Int. J. Quantum Chem. **5**, 359 (1971).
[8]R. J. Bartlett, C. E. Dykstra, and J. Paldus, in *Vectorization of Advanced Methods for Molecular Electronic Structure,* Proceedings of the NATO Advanced Research Workshop, edited by C. E. Dykstra, R. Ahlrichs, and W. Meyer (Reidel, Dordrecht, in press).
[9]J. Paldus, in *New Horizons of Quantum Chemistry,* edited by P.-O. Löwdin and B. Pullman (Reidel, Dordrecht, 1983), p. 31.
[10]V. Kvasnička, V. Laurinc, S. Biskupić, and M. Haring, Adv. Chem. Phys. **52**, 181 (1983); V. Kvasnička, V. Laurinc and S. Biskupić, Phys. Rep. **90**, 159 (1982).
[11]I. Lindgren and J. Morrison, *Atomic Many-Body Theory* (Springer, New York, 1982).
[12]R. J. Bartlett, Ann. Rev. Phys. Chem. **32**, 359 (1981).
[13]J. Čížek and J. Paldus, Phys. Scr. **21**, 251 (1980). J. Čížek, in *Quantum Theory of Polymers,* edited by J.-M. André, J. Delhalle, and J. Ladik (Reidel, Dordrecht, 1978), p. 103.
[14]H. Kümmel, K. H. Lührmann, and J. G. Zabolitzky, Phys. Rep. **36**, 1 (1978).
[15]J. Paldus and J. Čížek, Adv. Quantum Chem. **9**, 105 (1975); J. Paldus, *Diagrammatical Methods for Many-Fermion Systems* (University of Nijmegen, Holland, 1981).
[16]J. Paldus, J. Čížek, and I. Shavitt, Phys. Rev. A **5**, 50 (1972).
[17]A. P. Jucys, I. B. Levinson, and V. V. Vanagas, *Mathematical Apparatus of the Theory of Angular Momentum* (Institute of Physics and Mathematics of the Academy of Sciences of the Lithuanian S.S.R., Mintis, Vilnius, 1960) (in Russian). English translations by Israel Program for Scientific Translations, Jerusalem, 1962, and Gordon and Breach, New York, 1964; A. P. Jucys and A. A. Bandzaitis, *The Theory of Angular Momentum in Quantum Mechanics* (Institute of Physics and Mathematics of the Academy of Sciences of the Lithuanian S.S.R., Mintis, Vilnius, 1964) (in Russian); E. El Baz and B. Castel, *Graphical Methods of Spin Algebras in Atomic, Nuclear and Particle Physics* (Dekker, New York, 1972); see also Ref. 11.
[18]J. Paldus, J. Chem. Phys. **67**, 303 (1977).
[19]B. G. Adams and J. Paldus, Phys. Rev. A **20**, 1 (1979).
[20]J. Paldus, B. G. Adams, and J. Čížek, Int. J. Quantum Chem. **11**, 813 (1977); J. Čížek, Theor. Chim. Acta **6**, 292 (1966).
[21]Cf., e.g., B. G. Adams, K. Jankowski, and J. Paldus, Phys. Rev. A **24**, 2316 (1981).
[22]R. A. Chiles and C. E. Dykstra, J. Chem. Phys. **74**, 4544 (1981).
[23]R. J. Bartlett and I. Shavitt, Chem. Phys. Lett. **50**, 190 (1977), R. J. Bartlett, I. Shavitt, and G. D. Purvis, J. Chem. Phys. **71**, 281 (1979).
[24]J. Paldus, P. E. S. Wormer, F. Visser, and A. van der Avoird, J. Chem. Phys. **76**, 2458 (1982).
[25]Cf., e.g., Table VI of Ref. 21.
[26]K. Jankowski and J. Paldus, Int. J. Quantum Chem. **18**, 1243 (1980).
[27]B. G. Adams, K. Jankowski, and J. Paldus, Phys. Rev. **24**, 2330 (1981).
[28]R. A. Chiles and C. E. Dykstra, Chem. Phys. Lett. **80**, 69 (1981); S. M. Bachrach, R. A. Chiles, and C. E. Dykstra, J. Chem. Phys. **75**, 2270 (1981).
[29]R. Ahlrichs, H. Lischka, V. Staemmler, and W. Kutzelnigg, J. Chem. Phys. **62**, 1225 (1975).
[30]A. C. Hurley, *Electron Correlation in Small Molecules* (Academic, New York, 1976).
[31]W. Kutzelnigg, in *Methods of Electronic Structure Theory,* edited by H. F. Schaefer (Plenum, New York, 1977), p. 129.
[32]R. Ahlrichs, Comput. Phys. Commun. **17**, 31 (1979).
[33]V. Kvasnička, Phys. Rev. A **25**, 671 (1982).
[34]J. Paldus, M. Takahashi, and R. W. H. Cho, Int. J. Quantum Chem., Symp. (to be published).
[35]B. G. Adams and K. Jankowski, Int. J. Quantum Chem., Symp. **17**, 297 (1983).
[36]J. Paldus, P. E. S. Wormer, and M. Bénard, unpublished results.
[37]J. Paldus and M. J. Boyle, Int. J. Quantum Chem. **22**, 1281 (1982).
[38]J. Paldus, M. Takahashi, and R. W. H. Cho, Phys. Rev. B (to be published).
[39]R. W. H. Cho, M. Math. thesis, University of Waterloo, Canada, 1981.
[40]B. H. Brandow, Rev. Mod. Phys. **39**, 771 (1967).
[41]For the sake of simplicity we assume that $\hat{T}_1=0$. The monoexcited clusters may be easily included as well, obtaining the CCSD formalism if desired. See Ref. 19 for details.
[42]Cf., e.g., (a) J. Paldus, J. Čížek, and A. Laforgue, Int. J. Quantum Chem. **13**, 41 (1978); (b) J. Paldus, E. Chin, and M. G. Grey, *ibid.* **24**, 395 (1983).
[43]J. Čížek and J. Paldus, J. Chem. Phys. **47**, 3976 (1967).
[44]J. Paldus and J. Čížek, Phys. Rev. A **2**, 2268 (1970).
[45]J. Čížek and J. Paldus, Phys. Rev. A **3**, 525 (1971).
[46]R. J. Bartlett and G. D. Purvis, Phys. Scr. **21**, 255 (1980).
[47]M. Takahashi, J. Paldus, and J. Čížek, Int. J. Quantum Chem. **24**, 707 (1983).
[48]P.-O. Löwdin, Phys. Rev. **97**, 1509 (1955); J. Appl. Phys. (Suppl.) **33**, 251 (1962); Rev. Mod. Phys. **34**, 520 (1962); in *Quantum Theory of Atoms, Molecules and the Solid State* (Academic, New York, 1966), p. 601; Adv. Chem. Phys. **14**, 283 (1969).
[49]P.-O. Löwdin, *Symposium on Molecular Physics* (Maruzen, Tokyo, 1953), p. 13.
[50]R. Pauncz, *Alternant Molecular Orbital Method* (Saunders, Philadelphia, 1967).
[51]H. Fukutome, Prog. Theor. Phys. **40**, 998 (1968); **40**, 1227 (1968); **45**, 1382 (1971); **52**, 115 (1974); **52**, 1776 (1974); **53**, 1320 (1975); Int. J. Quantum Chem. **20**, 955 (1981).